Construction and Building Materials 487 (2025) 142023

Contents lists available at ScienceDirect

Construction and Building Materials

journal homepage: www.elsevier.com/locate/conbuildmat

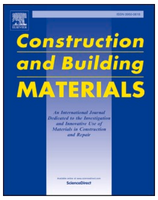

Alkali threshold level in concrete to trigger the alkali-silica reaction at simulated road pavement environments with alkali supply

Aneta Brachaczek [*,1], Mariusz Dąbrowski, Paweł Lisowski, Kinga Dziedzic, Michal A. Glinicki [*,2]

Institute of Fundamental Technological Research Polish Academy of Sciences, Pawinskiego 5b, Warsaw 02-106, Poland

ARTICLE INFO

Keywords:
Alkali-silica reaction
Alkali supply
Concrete durability
Critical alkali content
NaCl deicer
Reactive aggregate
Simulated service exposure conditions

ABSTRACT

To minimize the potential risk of concrete damage due to alkali-silica reaction (ASR) when using ordinary Portland cement in concrete mixtures, the alkali threshold level must be established for specific aggregate combinations. Since deicing salts used in the winter maintenance of highway structures can serve as an external source of alkalis, their impact on alkali threshold determination should be evaluated. An experimental investigation was conducted on concrete specimens subjected to a 60°C performance test, both with and without an external alkali supply. Concrete mixtures were prepared using Portland cements with alkali contents ranging from 0.45 % to 1.2 % Na_2O_{eq}. Mineral aggregates consisted of blends of potentially reactive coarse granite and natural siliceous sand, characterized by varying degrees of reactivity. The development of concrete expansion over time and associated changes in its dynamic elastic modulus, as well as the characteristics of ASR products in concrete is reported. The chemical reactivity index was determined based on the concentrations of Si, Ca, and Al in test suspensions containing aggregate, CaO, and NaOH. At simulated pavement environmental conditions variations in temperature and relative humidity in concrete were monitored. The effects of exposure conditions on expansion behavior and the composition of ASR products are discussed. The alkali threshold levels derived for such different exposure conditions are compared and analyzed in relation to the varying potential reactivity of fine aggregates.

1. Introduction

A sufficient alkalinity of the pore water solution (hydroxyl ion concentration) in concrete is considered as one of the principal conditions for chemical reactions with certain mineral constituents in rock aggregates. Alkali metal oxides (Na_2O, K_2O) in Portland cement clinker are the sources of the majority of Na^+ and K^+ ions and hydroxyl ions present in pore solution; some minor contribution may come from other constituents like supplementary cementitious materials, chemical admixtures or even some alkali-releasing aggregates [1–4]. A simplified relationship between the alkali content in cement, expressed in the sodium equivalent Na_2O_{eq}, the cement content in concrete mix and the hydroxyl ion concentration [OH^-] is described by a well known formula empirically developed by Helmuth et al. [5]. Taylor in [6] described a method for predicting the Na^+, K^+ and OH^- ions concentrations in the hydrated Portland cement pore solution based on minimum knowledge of the total Na_2O and K_2O content in cement. The experimental results confirmed reasonable agreement with the calculations. More recent measurements of alkalinity of pore solution in concrete performed by Hooton et al. [7] revealed that pore solution analysis can support fundamental research, contribute to the calibration of thermodynamic models, and assist in predicting long-term durability performance.

The term „alkali threshold level" [8] has been introduced to specify the nominal content of alkali in concrete which is sufficiently high to trigger the alkali-silica reaction (ASR). Such an alkali level should be determined for fine and coarse aggregate combination to minimise the potential risk of concrete damage due to ASR. The need and means to determine the alkali threshold (AT) (often called the maximum alkali loading) for aggregates have been discussed in the industry over many years [9–13]. In current technical standards a conservative approach is commonly adopted to specify a global alkali limit of 3.5 kg/m^3 or 3.0 kg/m^3 Na_2O_{eq}, using declared mean values of alkali content based on

---

* Corresponding authors.

E-mail addresses: aantolik@ippt.pan.pl (A. Brachaczek), mglinic@ippt.pan.pl (M.A. Glinicki).

[1] ORCID: 0000–0002-8272–4138

[2] ORCID: 0000–0001-5604–6954

https://doi.org/10.1016/j.conbuildmat.2025.142023
Received in revised form 11 May 2025; Accepted 28 May 2025

cement mill certificates, regardless of the aggregate. When using at least 8 % silica fume this threshold level additionally increases by a further 0.5 kg/m^3 Na_2O_{eq}. Following the approach adopted in ASTM C1778 [13] standard guide the specified AT level varies from 1.8 to 3.0 kg/m^3 Na_2O_{eq} depending not only on the aggregate reactivity level but also on the level of reliability required, related to the class of structure and its aggressive exposure conditions. The later factors include an expected contribution of external alkali sources, like seawater acting on marine structures or deicing salts sprayed on pavements for winter maintenance of roads and bridges, to increase the total alkali concentration in pore solution of concrete. Therefore the specified alkali threshold limit is lowered for such exposure conditions. However, the safety margin resulting from such an approach is not known.

A direct application of standard prism expansion test for determination of the alkali threshold for a concrete mix with ordinary Portland cement (CEM I according to EN 197–1 [14]) was proposed by Rønning et al. [15]. When expansion test results are plotted against the alkali content the intersection with a pre-determined expansion limit value (the test criterion, usually defined at 52 weeks of storage at 38°C) determines the critical alkali content level to trigger the deleterious alkali-silica reaction for the selected aggregate. A different, recently developed Alkali Threshold Test (ATT) to be completed in 21 days is supposed to allow for a determination whether the level of alkali in concrete is sufficient to trigger the ASR in the aggregates used [16]. This test method based on the T-FAST procedure specified in AASHTO TP144–23 [17] relies on the evaluation of a Reactivity Index (RI) determined using the concentration of Si, Ca and Al in the test suspensions of aggregate, CaO and NaOH. Coppens [18] critically reviewed the criteria for establishing the alkali threshold level aiming for a model calculation of critical level below which no ASR expansion may occur. The alternative threshold value was derived on the basis of an alkali concentration in the pore water of concrete of no more than 350 mM, especially aiming for concrete exposure conditions in waste disposal facilities protected from weather conditions. However, for concrete pavement engineering the environmental conditions and external alkali supply during the service life should be directly incorporated into the threshold evaluation procedure.

When sodium chloride is directly incorporated in concrete mix or when using sea water or sea sand [19], higher expansion and larger crack widths are observed with the increase of sodium ion concentration. Neither ATT nor the established concrete prism testing approach allow for evaluation of the influence of external alkali sources on the AT level. For such a purpose the RILEM AAR-12 performance test method with external alkali supply is proposed [20]. It is rather new test method and its significance still calls for a better understanding. In contrast to simple NaCl immersion tests this test method involves a cyclic environmental exposure to deicing salt solution and temperature variations to simulate traffic-environmental interaction. Such testing methodology is based on previous German field experience to detect and mitigate premature ASR-induced damages of concrete highway pavements, [21]. Using such a performance approach Giebson et al. [22] concluded that low alkali cements can delay ASR, but they cannot fully prevent it in concrete exposed to external sources of NaCl. They found that NaCl does not change pH of the pore solution, however it promotes direct dissolution of silica regardless of pH. Moreover, Przondziono et al. [23] demonstrated that cyclic mechanical loadings significantly affect the concrete microstructure. These degradation processes make it easier for liquids to penetrate the porous concrete, greatly increasing the likelihood of a more severe ASR development. In [24] the influence of concrete mix design on the ASR performance at cyclic exposure mimicking the fatigue traffic load, temperature variations and external NaCl solution exposure was studied. The effects of increased NaCl concentration and blended cement type (CEM I, CEM II/A-V and CEM II/B-S) on the ASR performance of concrete with certain aggregate combinations were revealed. However, the thermal and moisture conditions inside concrete specimens subjected to such a complex exposure were not studied. No published data is available on the influence of external NaCl solution exposure on the alkali threshold level relevant to concrete mix design for highway structures.

Table 1
The density, water absorption and potential reactivity of mineral aggregate.

Aggregate description, notation		Crushed granite	Natural fossil sand	Natural river sand	Natural fossil sand
			NR	MR	HR
Density$^{(1)}$ [Mg/m^3]	ρ_{rd}	2.57	2.62	2.66	2.65
	ρ_{ssd}	2.59	2.63	2.65	2.64
$WA_{24}^{(2)}$ [%]		0.9	0.3	0.4	0.4
AMBT$^{(3)}$ expansion [%]	14 days	0.19	0.09	0.3	0.36
	28 days	0.31	0.23	0.46	0.57

$^{(1)}$ ρ_{rd}—oven-dried particle density; ρ_{ssd}—saturated and surface-dried particle density;
$^{(2)}$ water absorption as per EN 1097–6 [28];$^{(3)}$ accelerated mortar bar test as per ASTM C 1260 [25]

The objective of this investigation is to establish the influence of external NaCl solution and simulated road pavement environments on the alkali threshold level for combined mineral aggregate in concrete. Aggregate combinations cover the blends of potentially reactive coarse granite and natural sands characterized by a range of reactivity degrees. The significance of RILEM AAR-12 test procedure is aimed to be better understood by monitoring the environmental conditions inside concrete specimens.

2. Experimental

2.1. Materials and specimens

Coarse aggregates, produced from crushed granite rocks of Polish origin were selected, with a maximum particle size of 16 mm. Three different natural sands (NR, MR, HR) with a maximum grain size of 2 mm were also utilized. Table 1 displays the characteristics of these aggregates, including expansion data obtained via the ASTM C1260 procedure [25]. An enlarged spectrum of fine aggregates was applied in order to explore the effects of employing local sands with varying levels of potential alkaline reactivity, ranging from non-reactive to highly reactive, as classified according to ASTM C 1778 [13].

Non-reactive sand (NR), predominantly consisting of quartz and feldspar, was collected from natural deposits in northeastern Poland, that have a long-term reputation of insensitivity to ASR. Petrographic analysis of quartz sand (MR) identified the presence of strained quartz, microcrystalline, and cryptocrystalline quartz, all indicative of reactivity potential. Reactive sand (HR), extracted from natural deposits in southern Poland, is primarily composed of quartzite fragments, with up to 20 % sandstone and 1 % granite. The degree of reactivity of sands was established in preliminary testing by accelerated mortar bar test (Table 1). Granite aggregate predominantly comprises quartz and feldspar, including alkali-feldspar and plagioclase. Petrographic analysis of coarse granite grains also revealed the presence of microcrystalline, cryptocrystalline, and strained quartz (Fig. 1), indicating potential reactivity. However, the AMBT expansion data in Table 1 is considered insufficient for definitive classification and also insufficient for classification of blends of such aggregate.

To encompass a range of alkali contents—from 0.45 % to 1.2 % Na_2O_{eq}—four types of Portland cement (CEM I, as per EN 197–1) were selected. Table 2 outlines the basic differences in cement properties and composition.

Air-entrained concrete mixtures were designed using the selected cements and aggregates, alongside other basic constituents listed in Table 3. No alkali boosting was applied. The target slump was set in the range from 100 to 160 mm, the fresh air content was set at 4–5 %. The

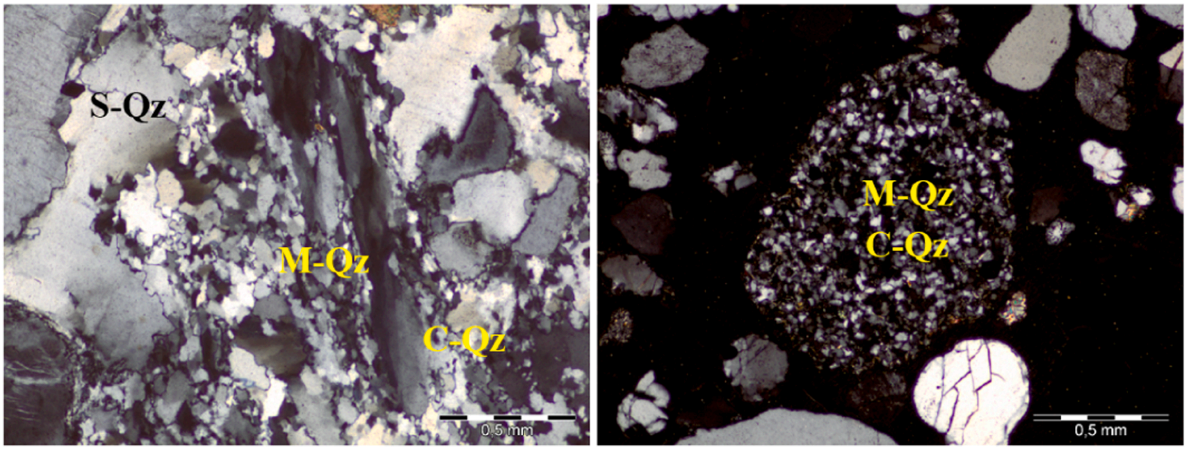

Fig. 1. Reactive forms of quartz in granite aggregate (a) and HR fine aggregate (b), M-Qz – micro-crystalline quartz, C-Qz – cryptocrystalline quartz, S-Qz – strained quartz.

Table 2
Portland cement properties and its alkali content (EN 196–2 [29], water-soluble – ASTM C114 [30]).

Properties	Cement identification			
	LA	MA	EA	HA
Alkali content Na_2O_{eq} [%]	0.36	0.68	0.88	1.2
Compressive strength [MPa] at				
2 days	20.4	25.8	28.5	28.6
28 days	53.0	57.5	57.8	61.5
Initial setting time [min]	195	174	220	238
Soundness [mm]	1	0.3	0.9	0.2
Specific surface area [cm^2/g]	3416	3749	3381	3895
Loss on ignition [%]	2.45	2.95	3.4	2.81
SO_3 content [%]	2.38	2.56	3.1	3.35
Water soluble alkali content Na_2O_{eq} [%] as per ASTM C114	0.20	0.43	0.69	1.05

Table 3
Concrete mixture design [kg/m^3].

Constituents and their contents	Performance testing on concrete prisms using:	
	60 °C test method - RILEM AAR-11 [31]	60 °C test method with alkali supply - RILEM AAR-12 [20]
Portland cement	360[b]	360[a]
Water	162	162
Quartz sand 0/2 mm	659[c]	659[c]
Crushed granite 2/ 8 mm	445	445
Crushed granite 8/ 16 mm	676	676
Air entraining admixture	0.18 to 0.6[d]	0.18 to 0.6[d]
Water reducing admixture	0.67 to 3.33[d]	0.67 to 3.33[d]

[a] quartz sand NR or HR -Table 1

[b] CEM I cements of different alkali content Na_2O_{eq} - according to Table 2

[c] quartz sand NR, MR or HR -Table 1

[d] the content adjusted for target fresh air content of 5 ± 1 % and slump of 130 ± 30 mm

fine (0–4 mm) and coarse (4–16 mm) aggregate contents constituted 45 % and 55 % of the total aggregate in the concrete mixture, respectively. The proportions of these constituents were selected to comply with standard specifications for road infrastructure construction in wet-freeze climate conditions [26]. Considering the exposure to deicing salts used in winter maintenance or lack thereof, the concrete mixtures were prepared for ASR performance testing with or without external alkali supply.

Concrete mixes were prepared in a laboratory mixer with a 50-liter capacity. The properties of the mixture, including slump, air content determined by the pressure method, and volumetric density, were determined according to EN 206 [27] standard procedures. Prismatic specimens (75x75x285 mm, three per series), equipped with stainless steel reference studs at the ends for length change measurement, were produced in laboratory conditions (the temperature of 20–22°C and RH 65 ± 5 %) using a vibration table for mixture compaction. Cubic specimens (100 mm sides) were cast for compressive strength tests. Following mold removal, the specimens were cured under moist conditions, adhering to relevant standards.

2.2. Test methods

The ASR performance of air-entrained concrete containing coarse granite aggregate was evaluated without and with alkali supply using a 60 °C concrete prism test as per RILEM AAR-11 [31] and RILEM AAR-12 [20] procedures, respectively. Using the reference procedure without alkali supply the concrete specimens were exposed to high humidity environmental conditions at the temperature of 60 °C with the use of dedicated stainless-steel containers and condensate reactor allowing for environmental humidity to be close to 100 % RH, for at least 20 weeks. Periodically the length of specimen, its mass and the elastic resonance frequency were measured over a 20-week exposure time. GrindoSonic MK5 device was used to determine the resonant frequency of flexural vibrations and the dynamic elastic modulus of concrete as per ASTM C215 [32].

RILEM AAR-12 test method simulates the de-icing salt exposure along with fatigue effects on road pavements by exposing concrete specimens to cyclic temperature and moisture variations. Initially, concrete specimens undergo a 28-day curing and conditioning period. Subsequently, they are subjected to at least 10 test cycles, each lasting 2 weeks, which include the following steps: 5 days in a laboratory heating chamber with forced ventilation at 60 ± 5°C, 2 days of saturation in a 3 % NaCl solution at 20 ± 2°C, 6 days in a sealed steel container in a thermostatic water condensate chamber at 60 ± 2°C and RH > 98 %, followed by 1 day of stabilization in a closed container at 20 ± 2°C and RH > 98 %. At the end of each cycle, the length and mass of the specimens, as well as the elastic resonance frequency, are measured. Additionally, using extra concrete specimens prepared with the same procedure (cement LA, sand NR), the internal temperature and humidity conditions were monitored during AAR-12 exposure cycles. For this purpose the holes of 20 mm in diameter were drilled in hardened specimens and subsequently two measuring devices were applied - iButon sensors and Vaisala probe (Appendix 1). The temperature/RH

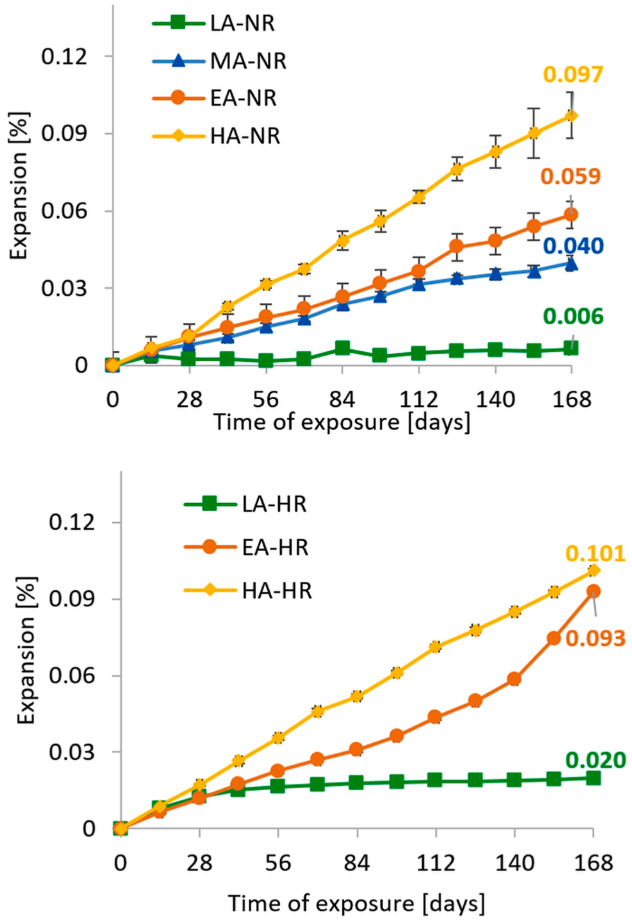

Fig. 2. Expansion of concrete specimens during RILEM AAR-12 test exposure using 3 % NaCl solution: a) NR sand, b) MR sand, c) HR sand.

monitoring method was based on previously gained experience reported in [33,34].

From the measurements obtained without and with alkali supply, the expansion (ε), mass increase (ΔM), and the change of dynamic elastic modulus (ΔE_{dyn}) of concrete were calculated in respect to the initial values. Upon termination of standard exposure period, the microstructure of concrete was examined using a scanning electron microscope (SEM) with energy-dispersive spectroscopy (EDS) for micro-area analysis. Concrete prisms were cut into 25 × 40 × 10 mm specimens, dried for 3 days at 50°C, and impregnated with epoxy resin. The specimens were then ground on diamond discs and polished using diamond pastes. After surface preparation specimens were sputtered with a 20 nm carbon layer. Microstructural observations were conducted using a JEOL JSM6460LV microscope equipped with an energy-dispersive X-ray spectral analysis (EDS) detector. The SEM operated with an acceleration voltage of 20 kV and a working distance of 10 mm.

For the residual flexural strength determination the standard EN 206 test procedures were used. For the alkali threshold determination using the reactivity index in the system under varying alkali loadings the AASHTO TP 416 [35] procedure was applied. The concentrations of silicon, calcium, and aluminium ions were analyzed using an ICP-OES PerkinElmer Optima 5300 DV spectrometer, calibrated with standards specific to each element. Before analysis, the specimens were acidified with 2 % HNO_3 and each measurement was performed in triplicate to ensure accuracy.

3. Results

3.1. Expansion and elastic properties

The results of concrete expansion, dynamic elastic modulus and change of mass of specimens as per RILEM AAR-12 test procedure are shown in Figs. 2 and 3 and in Table 4. The initial average values of dynamic modulus of elasticity, calculated from the measured resonance frequencies, were within the range from 35.6 to 41.9 GPa. The dispersion of elastic properties data was low – the coefficient of variation for each series of specimens was less than 2.5 %.

The results of the expansion and change in the elastic modulus of concrete were strongly dependent on the alkali content in the cement used. The highest expansion and strongest decrease in elastic modulus were observed in concrete with high alkali content cement (HA), with expansion ranging from 0.83 % to 1.16 % and a decrease in elastic modulus from 13.0 % to 26.8 % after 10 cycles. The use of low alkali cement (LA) significantly impeded the expansion development in time, causing the reduction of final expansion by about a range of magnitude: down to the range from 0.06 % to 0.19 %. Additionally, in most cases, a slight increase in elastic modulus of up to 2.5 % was observed. Concrete with medium (MA) and elevated (EA) alkali content cement exhibited elevated expansions ranging from 0.31 % to 0.35 % and from 0.45 % to 0.58 %, respectively. Extending the test duration by another 2 cycles (4 weeks) did not slow the expansion development nor reduction of elastic modulus rate, it progressed at a similar rate.

For each type of fine aggregate used in concrete an increase of alkali loading resulted in increased expansion rate and reduced deterioration rate of elastic modulus. Concrete specimens with reactive sand HR exhibited higher expansion than concrete specimens with NR and MR

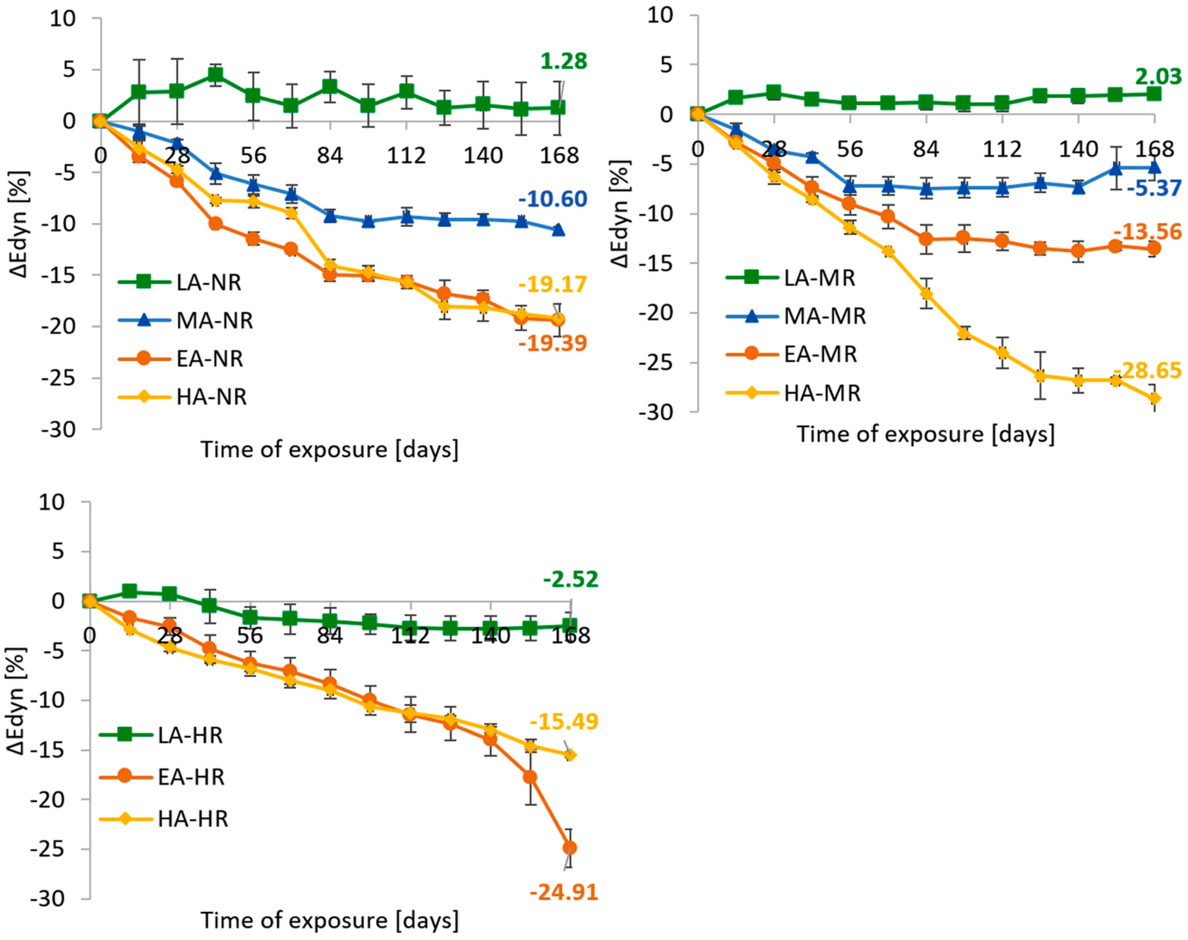

Fig. 3. Change of dynamic elastic modulus of concrete during RILEM AAR-12 test exposure using 3 % NaCl solution: a) NR sand, b) MR sand, c) HR sand.

Table 4
Final expansion, dynamic elastic modulus, change of mass (average value ± standard deviation) according to RILEM AAR-12 test procedure after 10 cycles (20 weeks of exposure).

Concrete mix		ε [%]	ΔE_{dyn} [%]	E_{dyn} [GPa]	Δm [%]
Cement type	Sand type				
LA	NR	0.006 ± 0.001	1.55 ± 2.32	39.49 ± 0.14	1.13 ± 0.09
MA		0.035 ± 0.002	−9.5 ± 0.56	33.01 ± 0.42	1.61 ± 0.15
EA		0.048 ± 0.003	−17.33 ± 0.85	31.38 ± 0.24	1.51 ± 0.00
HA		0.083 ± 0.006	−18.16 ± 1.33	31.69 ± 0.73	1.26 ± 0.07
LA	MR	0.009 ± 0.002	1.82 ± 0.74	39.24 ± 0.94	1.18 ± 0.12
MA		0.031 ± 0.002	−7.31 ± 0.63	35.21 ± 0.28	1.29 ± 0.09
EA		0.045 ± 0.003	−13.81 ± 1.07	32.56 ± 0.24	1.32 ± 0.05
HA		0.116 ± 0.009	−26.80 ± 1.21	26.52 ± 0.32	1.50 ± 0.05
LA	HR	0.019 ± 0.001	−2.73 ± 1.27	34.62 ± 0.67	1.47 ± 0.06
EA		0.058 ± 0.001	−13.98 ± 1.63	33.90 ± 0.81	1.13 ± 0.14
HA		0.085 ± 0.001	−12.95 ± 0.32	34.20 ± 0.24	1.13 ± 0.03

sands, except the case of high alkali cement HA when the highest expansion was noted for MR sand. In most cases the relative expansion differences induced by NR and MR sands were small. As seen from Table 4 the cyclic exposure of specimens to temperature/moisture environmental changes and NaCl solution soaking resulted in rather consistent mass increase, finally reaching 1.1–1.6 %. No clear effects of sand reactivity nor the type of cement on the mass changes were observed.

The development of the internal temperature and relative humidity in concrete during AAR-12 exposure is presented in Fig. 4 (in the center of the specimen) and in more details in Appendix 1. The temperature measurements obtained with iButton sensors and Vaisala probes demonstrated the expected changes during the four stages of exposure. Recorded temperature history at the depth of 1/2 of the specimen thickness is well fitting the specified temperature limits. The RH measurements with iButton at the depth of 37 mm demonstrate a gradual RH decrease during drying phase. During the transition from NaCl solution the RH is reduced to about 90 % and later it very slowly increases up to 98 %. The prevailing RH during the specimen storage in the container in condensate reactor is within the range 94–97 %. The closed container transition from the 60 °C reactor to 22°C laboratory environment resulted in data out of the range of measurements. In measurements taken by Vaisala probes during the drying stage the RH reduces from 95 % to about 65–69 %, during the soaking stage goes up to 95 % and the end of the cycle stays at the level of 97 %. Based on the conducted humidity measurement experiment, it was found that the humidity inside the sample was maintained at a high level throughout the entire process, despite the drying stage.

In Fig. 5 and Table 5 the results of expansion measurements, dynamic

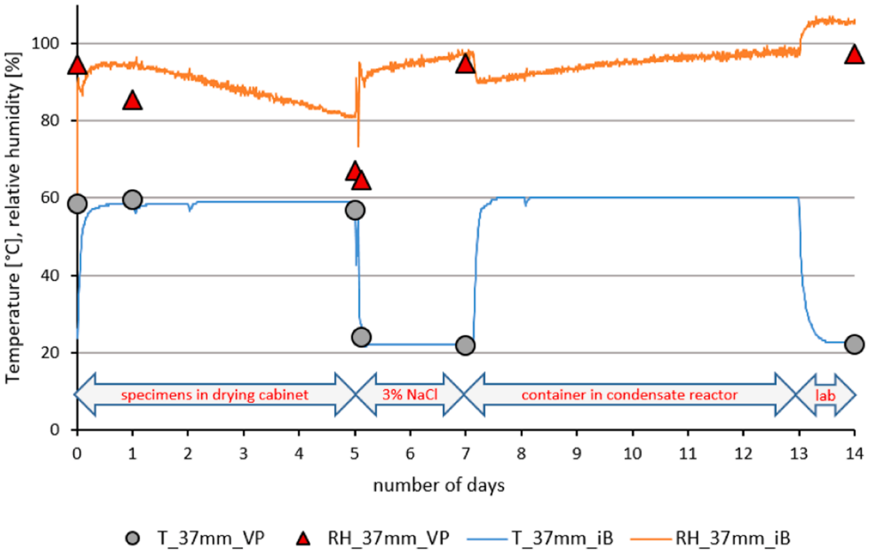

Fig. 4. Temperature and relative humidity in concrete at the depth of 37 mm recorded during the first test cycle of RILEM AAR-12 procedure (VP-Vaisala probe, iB-iButton).

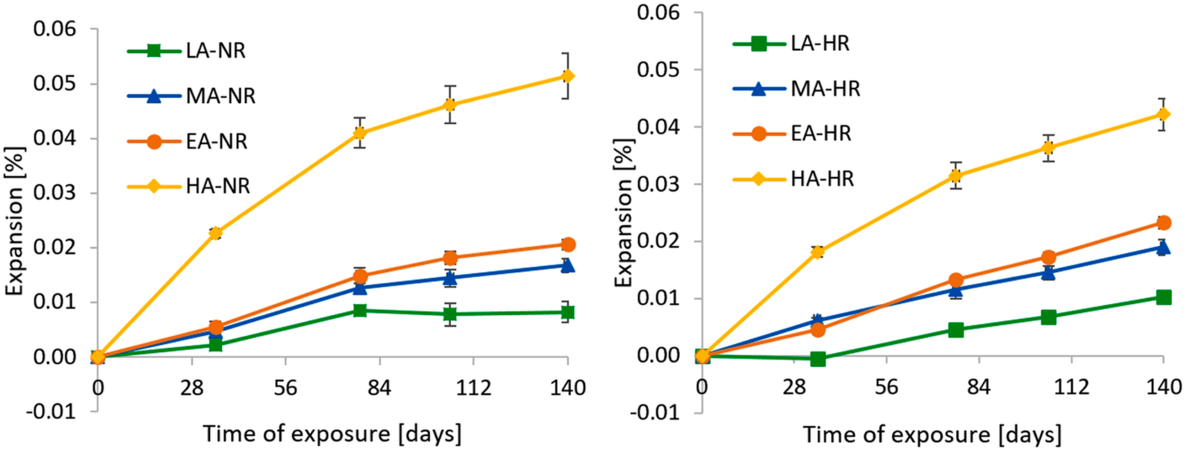

Fig. 5. Expansion of concrete during RILEM AAR-11 test exposure: a) NR sand, b) HR sand.

Table 5
Final expansion, dynamic elastic modulus, change of mass (average value ± standard deviation) according to RILEM AAR-11 test procedure after 20 weeks of exposure.

Concrete mix		ε [%]	ΔE$_{dyn}$ [%]	E$_{dyn}$ [GPa]	Δm [%]
Cement type	Sand type				
LA	NR	0.008 ± 0.002	−3.45 ± 0.34	40.49 ± 0.21	−0.07 ± 0.04
MA		0.017 ± 0.001	−3.58 ± 0.34	32.43 ± 0.25	−0.04 ± 0.03
EA		0.021 ± 0.001	−1.23 ± 0.64	36.58 ± 0.51	0.16 ± 0.02
HA		0.051 ± 0.004	−0.04 ± 0.99	37.94 ± 0.89	0.51 ± 0.03
LA	HR	0.010 ± 0.001	2.91 ± 0.36	42.99 ± 0.57	0.01 ± 0.07
MA		0.019 ± 0.001	−0.06 ± 0.30	35.05 ± 0.49	−0.17 ± 0.04
EA		0.023 ± 0.001	0.58 ± 0.73	39.30 ± 0.22	0.18 ± 0.02
HA		0.042 ± 0.003	3.72 ± 1.05	36.02 ± 0.71	0.46 ± 0.03

elastic modulus and mass change obtained for concrete specimens in RILEM AAR-11 exposure are presented. The applied environmental exposure conditions (the temperature of 60 °C, close to 100 % RH) serve here as the reference environment for comparison with the external alkali supply environment.

The kinetics of expansion observed for concrete specimens made with HA cement was high regardless the reactivity of sand used in aggregate mixture. The shape of expansion-time curves was typical for reactive aggregate concrete prism tests without alkali supply. The decreasing content of alkalis in cement was consistently reflected by a decrease of expansion. For LA and MA cements the average final expansion of concrete was below 0.02 %, while for higher alkali contents in cement the expansion reached the range up to 0.05 %.

The observed changes in dynamic elastic modulus were negligible, in average within the range from −3.4 % to + 3.7 %. For HR sand concrete series even a little increasing tendency during the test exposure was observed. The relative mass changes brought by AAR-11 exposure conditions were also negligible - in average within the range from −0.1 % to + 0.5 %.

Apart from expansion differences, the AAR-11 and AAR-12 test exposure resulted in distinct differences in the residual flexural strength of concrete. The flexural strength of concrete prisms post-AAR-11 testing

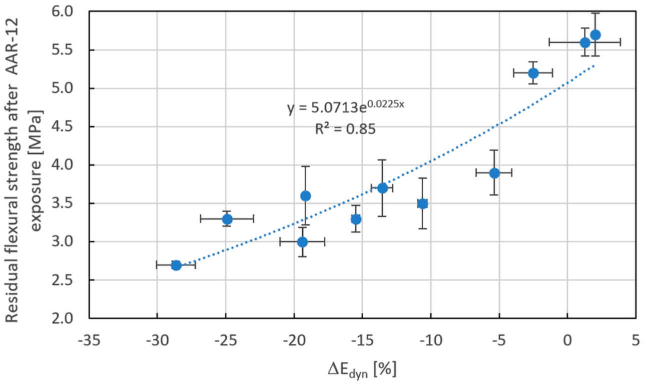

Fig. 6. The relationship between residual flexural strength and dynamic elastic modulus change of specimens exposed to RILEM AAR-12 conditions.

ranged from 4 to 5.8 MPa, while for AAR-12 tested specimens, it ranged from 2.7 to 5.7 MPa. Unlike AAR-12, AAR-11 test results showed no correlation between specimen expansion, dynamic elastic modulus, and flexural strength. However, for specimens exposed to AAR-12 test conditions the changes in dynamic elastic modulus and the residual flexural strength were observed to increase for increased expansion of specimens. The best empirical description of the observed trend is shown in Fig. 6. This finding aligned with surface crack observations on external surfaces of samples, as the AAR-12 samples exhibited abundant cracks linked to high expansion levels. The comparison of ΔE_{dyn} and Δm data in Tables 4 and 5 revealed that the AAR-12 test conditions led to significantly greater concrete damage than in AAR-11. These effects were clearly reflected in the residual strength of specimens, emphasizing the increased impact of simulated pavement environments on ASR-induced damage.

3.2. *SEM-EDS observations of reaction products*

In the cross sections of specimens subjected to SEM examination after termination of RILEM AAR-12 exposure (with alkali supply) the products of alkali-silica reaction were abundantly present. ASR products were predominantly detected in the cracks within coarse granite aggregate, Figs. 7 and 8. The extent of concrete expansion due to ASR was associated with increased structural damage, as ASR products were also found in the interfacial transition zone (ITZ) between the aggregate and the cement matrix, as well as within the cement matrix and air voids, Fig. 9. The abundance of ASR products was influenced by the alkali content in cement used; the highest abundance was observed in concrete made with HA cement. Conversely, concrete prepared with LA cement showed only a few instances of ASR products within coarse aggregate, with notably thinner cracks. Both crystalline and amorphous ASR products were found in the coarse aggregate, with the amorphous form (characterized by a higher Na/K ratio) being more prevalent. Furthermore, in concrete with nonreactive sand NR, no ASR signs were present in the sand grains. However, in concrete with reactive fine aggregate, numerous sand grains were partially or fully converted into ASR products, Fig. 10. Both Friedel's salts and ettringite were found in the cement matrix. However, the presence of Friedel's salts was very small and therefore considered negligible, Fig. 11.

The composition of ASR products was evaluated by EDS in micro-areas using the atomic ratios Ca/Si, (Na+K)/Si and Na/K. The results presented in Table 6 show, after taking into account the standard deviation, similar alkali contents (Na+K)/Si in ASR products in granite grains 0.22–028 in average, regardless of the exposure type. In amorphous ASR products in aggregate grains Ca/Si ratios were mostly in the respective ranges 0.29–0.37 and 0.26–0.30, suggesting higher calcium content under AAR-12 than AAR-11. It was noted that in the AAR-12 exposure specimens with high-alkaline cement HA, a higher content of potassium ions was found compared to sodium in ASR products. In the samples made using the other cements, a higher content of sodium than potassium was found. Na/K ratios under AAR-11 exposure conditions were much lower, i.e. within the range from 0.12 to 0.23 in average. The HA-NR sample showed the presence of a crystalline gel which showed a slightly higher alkali content compared to the amorphous gel.

Results of similar examination of cross sections of specimens after termination of RILEM AAR-11 exposure (without alkali supply) are shown in Figs. 12–14 as well as in Table 6.

The alkali-silica reaction products observed in the specimens exposed to RILEM AAR-11 test conditions were entirely amorphous. Notably, in the specimens with the highest expansion following the AAR-11 test, cracks filled with ASR gel were observed, with widths reaching up to 15 μm. In concrete specimens containing reactive HR sand, no sand grains were partially or fully converted into ASR products. Furthermore, there was no significant presence of ASR products in the cement matrix, with only a few isolated cases. The chemical composition of ASR products after AAR-11 test exposure was similar to these after AAR-12 test (Table 6).

Surface cracking observations aided with digital handheld microscope on specimens after AAR-12 and AAR-11 test exposure showed a significant influence of cyclic changes in temperature, humidity and external access of NaCl on the presence and width of surface cracks. Cracks observed in the AAR-12 specimens were abundant and up to

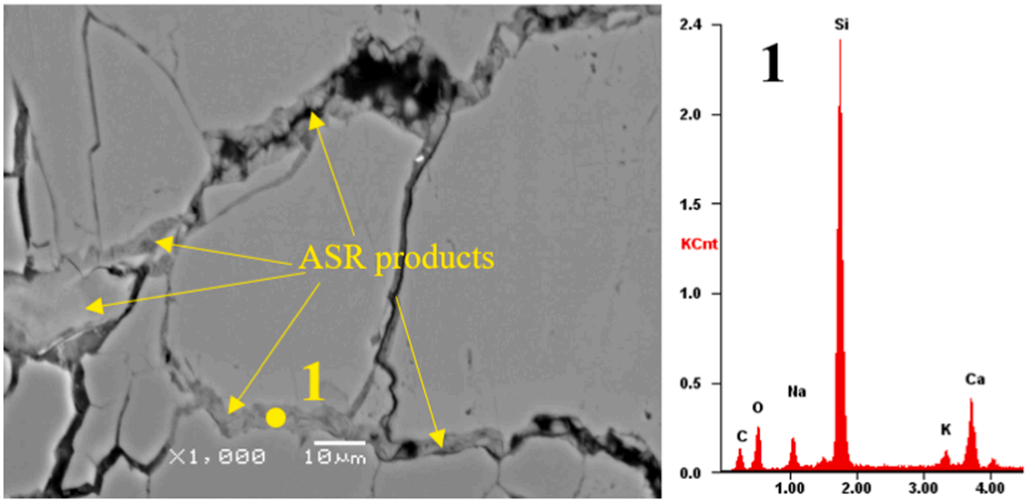

Fig. 7. ASR products in cracked granite grain in LA-HR concrete, (1) ASR product.

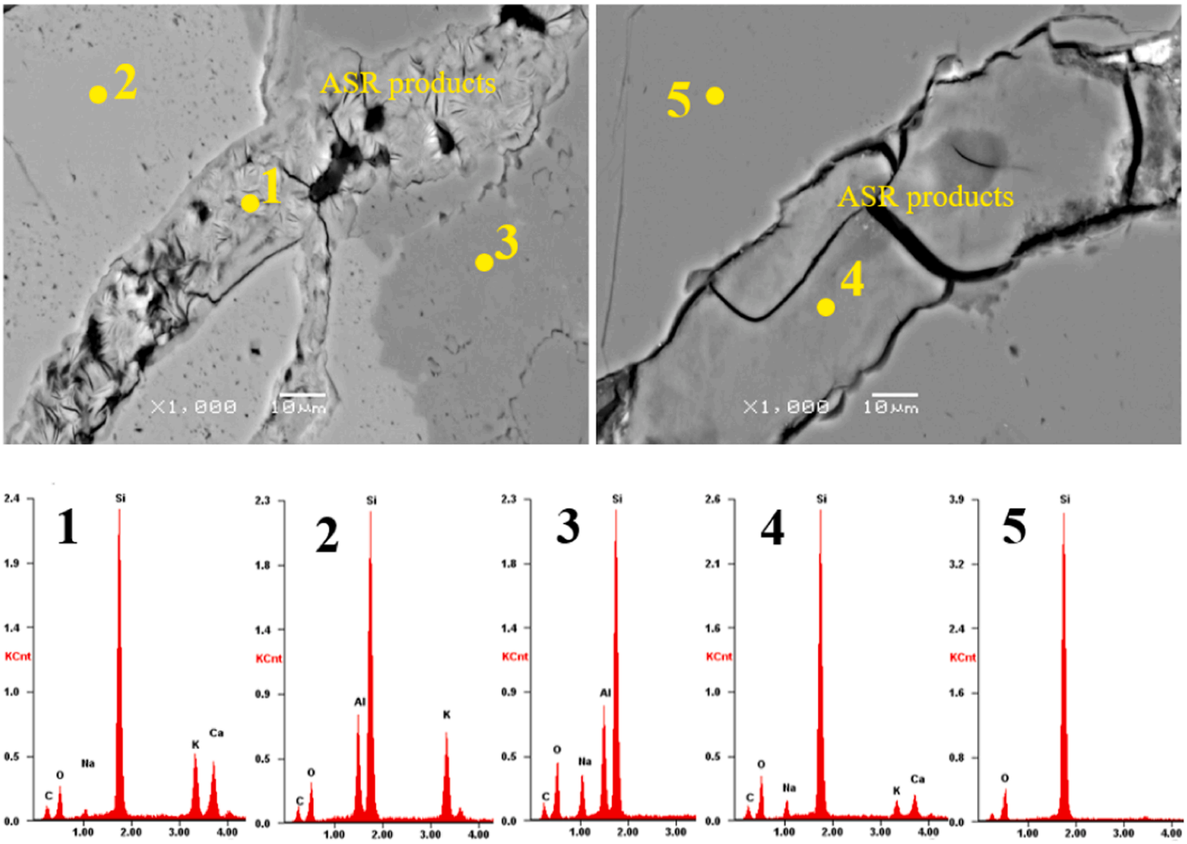

Fig. 8. Crystalline (1) and amorphous (4) ASR products in cracked granite grain in HA-NR concrete, (2) potassium feldspar, (3) sodium feldspar, (5) quartz.

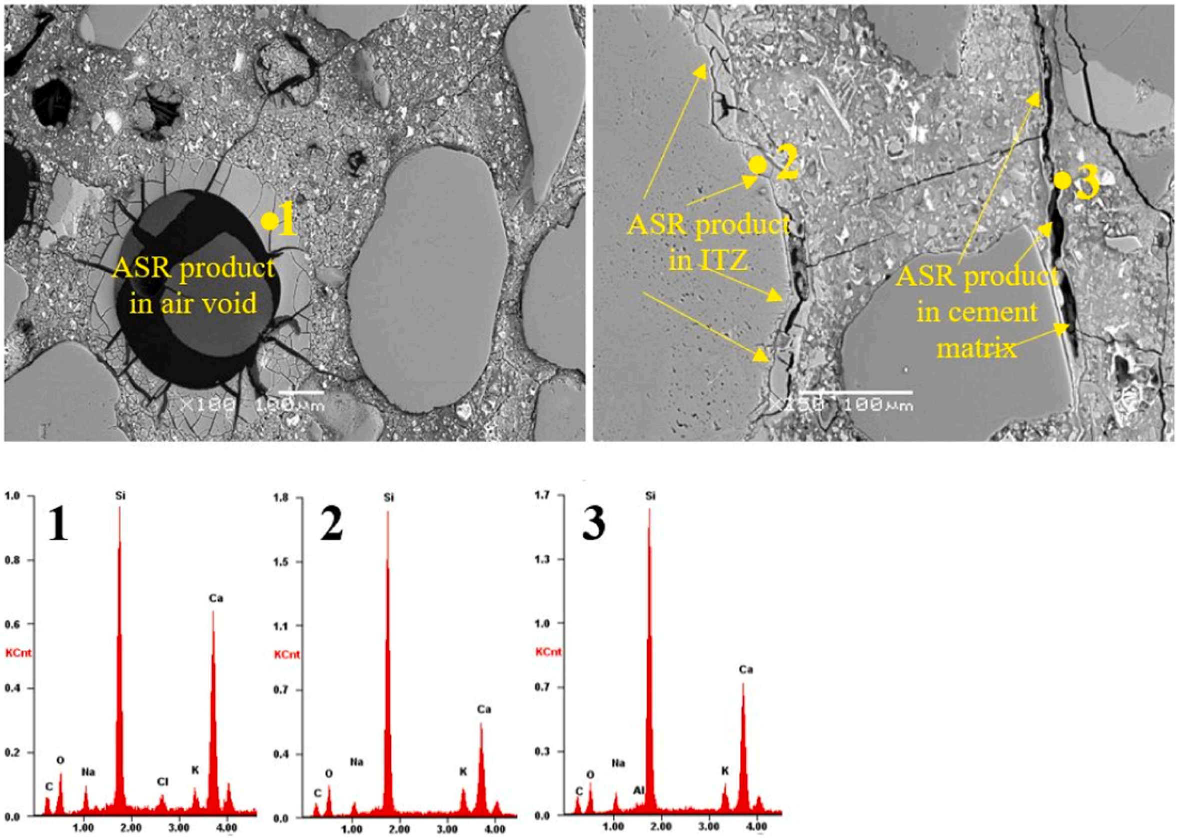

Fig. 9. ASR products in air void (1), interfacial transition zone (2) and cement matrix (3) in HA-NR concrete.

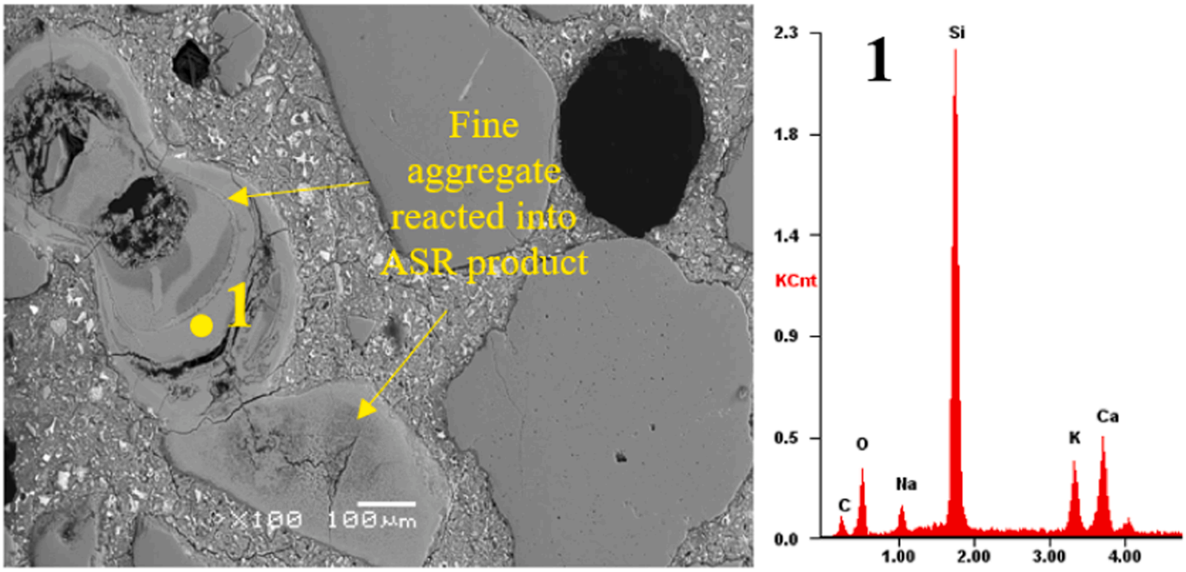

Fig. 10. SEM image of sand grain fully reacted into ASR product in HA-HR concrete.

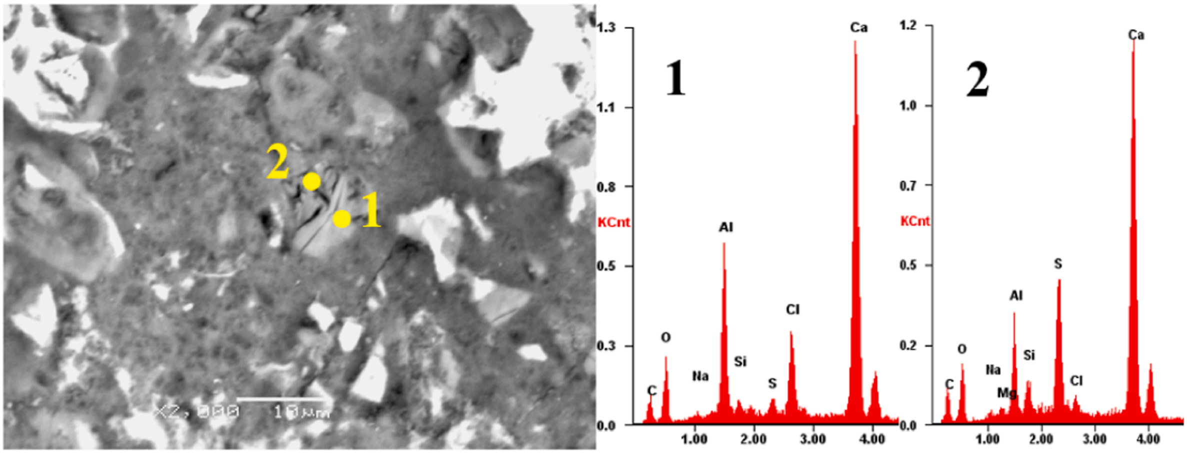

Fig. 11. SEM image of cement matrix in HA-HR concrete, (1) Friedel's salt, (2) ettringite.

Table 6
Chemical composition of ASR products in concrete after RILEM AAR-12 and AAR-11 exposure.

Reaction products		Concrete specimens designation					
Location	Composition indicator	**MA-NR**	**EA-NR**	**HA-NR**	**LA-HR**	**EA-HR**	**HA-HR**
RILEM AAR−12 exposure (with alkali supply)							
Amorphous ASR products in granite grains	Ca/Si	0.26 ± 0.08	0.37 ± 0.08	0.29 ± 0.09	0.33 ± 0.09	0.37 ± 0.11	0.37 ± 0.11
	(Na+K)/Si	0.26 ± 0.08	0.22 ± 0.06	0.28 ± 0.04	0.23 ± 0.02	0.25 ± 0.06	0.25 ± 0.06
	Na/K	1.14 ± 0.6	1.37 ± 0.46	0.91 ± 0.38	2.64 ± 1.33	1.38 ± 0.52	0.41 ± 0.22
Crystalline ASR products in granite grains	Ca/Si	nt	nt	0.27 ± 0.02	nt	nt	nt
	(Na+K)/Si	nt	nt	0.34 ± 0.02	nt	nt	nt
	Na/K	nt	nt	0.20 ± 0.05	nt	nt	nt
Fully or partially reacted sand grain	Ca/Si	nt	nt	nt	nt	nt	0.27 ± 0.08
	(Na+K)/Si	nt	nt	nt	nt	nt	0.32 ± 0.04
	Na/K	nt	nt	nt	nt	nt	0.59 ± 0.10
RILEM AAR−11 exposure (without alkali supply)							
Amorphous ASR products in granite grains	Ca/Si	nt	nt	0.30 ± 0.04	nt	0.30 ± 0.04	0.26 ± 0.04
	(Na+K)/Si	nt	nt	0.24 ± 0.07	nt	0.27 ± 0.03	0.24 ± 0.05
	Na/K	nt	nt	0.12 ± 0.6	nt	0.23 ± 0.08	0.16 ± 0.08

nt-not tested

250 µm wide, while in the AAR-11 specimens very few cracks were observed, mainly with a width of up to 20 µm, Fig. 15.

3.3. Reactivity index measurements

The measured concentration of the silicon, calcium and aluminium in each solution from different alkali loading levels was used to calculate

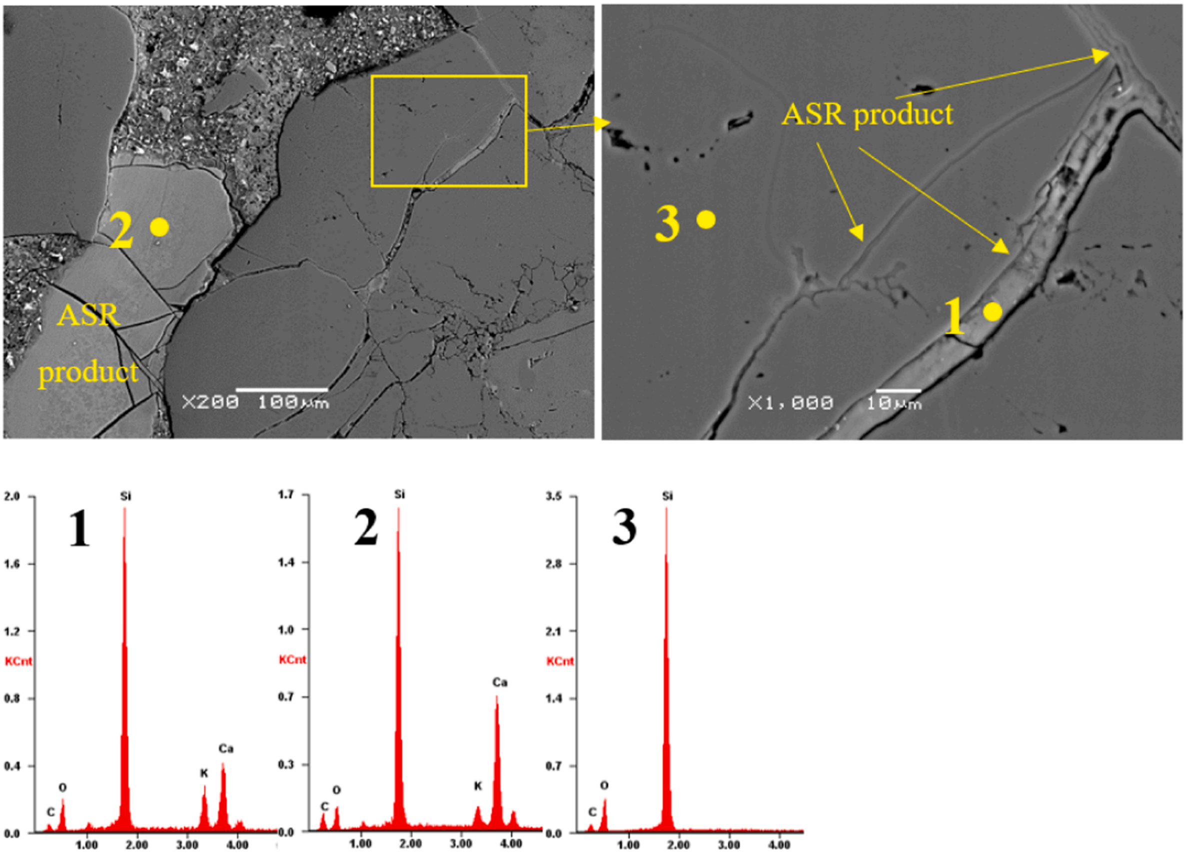

Fig. 12. Amorphous ASR products in granite grain (1) and cement matrix (2) in concrete HA-NR after AAR-11 test exposure, (3) quartz.

the reactivity index RI according to the formula [35]:

$RI = [Si] / ([Ca] + [Al])$

where

Si – concentration of silicon in milimoles per liter,

Ca – concentration of calcium in milimoles per liter,

Al – concentration of aluminum in milimoles per liter.

The resulting reactivity index (Table 7, Fig. 16) is seen increasing for increasing the alkali content in solution. The dispersion of data from the average values was not more than 23 %, except the measurements for the lowest alkali content exhibiting elevated dispersion. According to [35] all reactive aggregates are classified into two types: Type A and Type B based on the aluminum concentrations in the liquid phase. If the average concentration of silicon measured in the three filtered solutions is > 1 mM and the aluminum concentration is > 0.2 mM, the aggregate is designated as a Type A aggregate. Following this classification the tested granite aggregate was type A, therefore for the determination of the alkali threshold the criterion of RI= 0.45 (the dashed line) should be relevant. However, the resulting alkali threshold cannot be determined because the results of all tested solutions showed RI above the suggested limit of 0.45.

4. Analysis and discussion

The expansion data evaluation is based on the relationship between the alkali loading in concrete mix and final expansion of specimens, as shown in Figs. 16 and 17. Following the French and Swiss specifications ([31] Annex C, [36]) the limiting expansion value for deleterious reaction in concrete is assumed as 0.02 % after 20 weeks of exposure in RILEM AAR-11 environment. An analogous expansion limit of 0.03 % after 10 cycles (20 weeks of exposure) is assumed for RILEM AAR-12 exposure [21,26]. With these expansion criteria the AT limits are established for two considered environmental exposure conditions. For no alkali supply conditions (Fig. 17) the AT is 2.7 or 2.9 kg/m^3 Na_2O_{eq} for concrete containing HR or NR sand, respectively. The difference in the alkali threshold limit brought by such a change of sand reactivity is quite small. With alkali supply conditions (Fig. 18) the AT limit is 1.8 or 2.25 kg/m^3 Na_2O_{eq} for concrete containing HR or NR sand, respectively. Such a limit for MR sand concrete (2.35 kg/m^3 Na_2O_{eq}) is slightly higher than for HR. The comparison of established alkali thresholds shows their much larger sensitivity to sand reactivity when concrete is exposed to alkali supply conditions. Moreover, the AT is significantly lowered for alkali supply conditions when reactive HR sand is used as a constituent of concrete mix. This is not the case when nonreactive sand is used.

If the water-soluble alkalis are considered instead of total alkalis in cement (Table 2), the AT might be expressed in terms of water soluble alkali content. Accordingly, such water soluble AT levels are lower than those shown in Figs. 17–18, i.e. 2.0–2.2 kg/m^3 Na_2O_{eq} for no alkali supply, from 1.4 to 2.1 kg/m^3 Na_2O_{eq} for alkali supply conditions. The water-soluble alkalis are more readily available to react with other components in the cement mixture [37]. Thus such an approach could enhance the accuracy of AT determination and adequate cement selection, however, concrete prism tests suffer from some uncontrolled alkali leaching, so the advantage gained might be lost. According to Borchers [38] Portland cements should continue to be selected based on the total Na_2O equivalent, because of a strong linear correlation with the hydroxide ion concentration in pore solution.

Considering the significance of the actual alkali concentration in the pore solution [4], particularly under alkali supply, the authors attempted to use in-situ leaching test method [39]. Unfortunately, due to extensive cracking in concrete subjected to AAR-12 exposure the saturation conditions could not be met and the test was unsuccessful. Possible leaching of portlandite during immersion of concrete in NaCl solution could diminish its availability for ASR products formation. However, this has not been confirmed by the current results on reaction

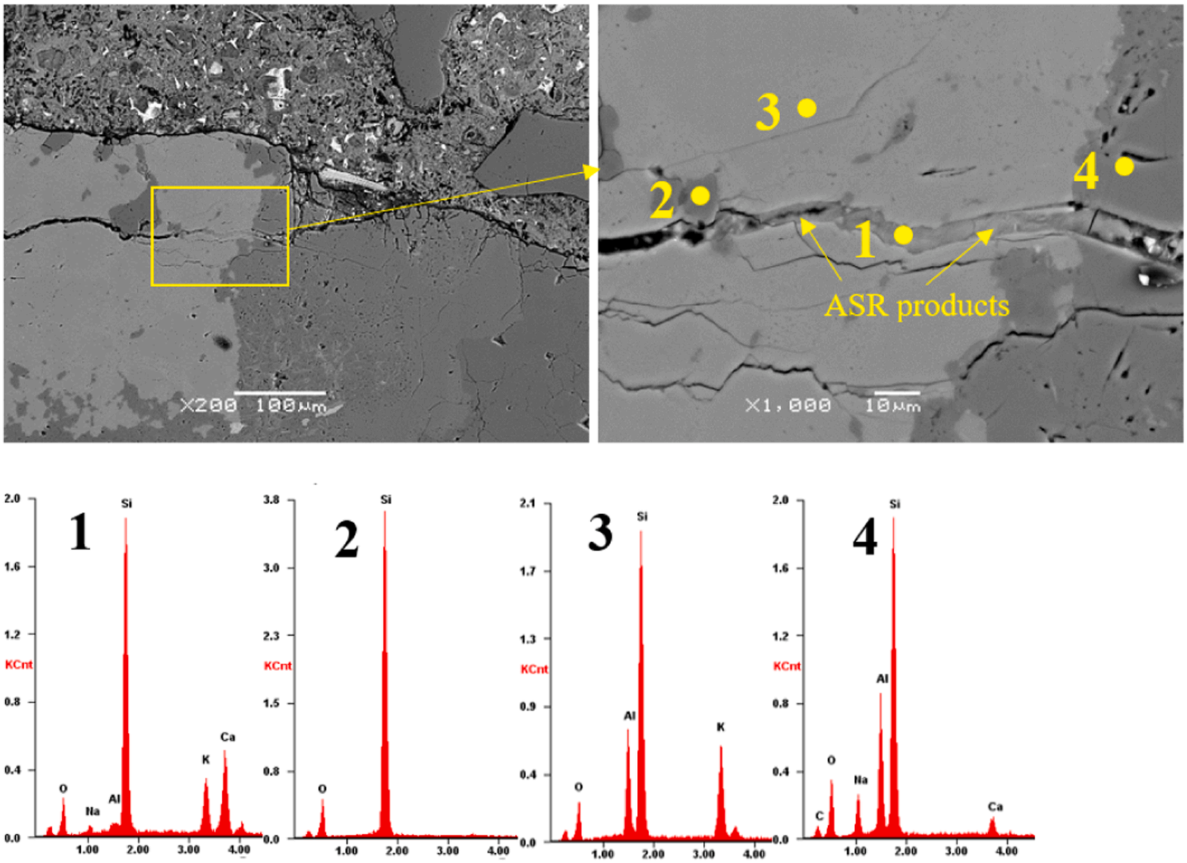

Fig. 13. Amorphous ASR products in granite grain (1) in concrete EA-HR after AAR-11 test exposure, (2) quartz, (3) potassium feldspar, (4) sodium-calcium feldspar.

products composition. The expansion of concrete prisms exposed to 60 °C is known to be influenced by the rate and amount of alkali leaching [40]. Some alkali leaching is also expected in the surface layer of concrete pavements exposed to moist environments. The 60°C test evaluation criteria applied in several European countries, eventually taking into account a potential variability of alkali content due to leaching, were verified in long term practice in respect to existing structures. Therefore the current test evaluation is based on these criteria. However, the problem of alkali leaching remains challenging for evaluation of accelerated ASR laboratory tests.

A desired comparison of the alkali threshold determined on the expansion data (Figs. 17 and 18) with the alkali threshold determined using the reactivity index (Fig. 16) is not available. RI consistently exceeded the critical value of 0.45 for all alkali loadings, however the increased data scatter should be noted. The reactivity of analyzed granite aggregate fails to meet the North American criteria for establishing AT [35]. Consequently, the AT determination for such aggregate combination must be based on concrete expansion data, as proposed in this investigation.

The observed reduction of AT for simulated pavement environments with alkali supply conditions could not be supported with the alkali penetration data. Detection of small changes of sodium concentration in cement paste in concrete cross-sections is usually beyond a detection range EDS analysis systems [41]. Only few published experiments with alkali supply could provide the sodium penetration profiles obtained with LIBS technique [42,43]. Moreover, the LIBS results were found to be highly influenced by the alkali metal presence in certain mineral aggregates. Therefore the meaningful determination of Na penetration profile in concrete exposed to external NaCl solution still remains challenging.

The influence of environmental conditions on the alkali threshold limit for air entrained concrete containing a particular blend of mineral aggregate cannot be confronted with literature data since they are not available. The observed sensitivity to sand reactivity when concrete is exposed to alkali supply is confirmed by substantially larger abundance of ASR reaction products present in concrete. The interaction of reactivity of HR sand with reactivity of granite aggregate displayed by the expansion increase is associated with the occurrence of ASR products also in sand grains. Some sand grains were fully converted into ASR products, as shown in Fig. 10. Moreover, in contrast to merely amorphous reaction products observed without alkali supply, both crystalline and amorphous products were present at alkali supply conditions. The composition of reaction products characterized by two atomic ratios (Na+K)/Si and Ca/Si is illustrated in Fig. 19. Such characteristics of ASR products generally fits well to the range of composition reported in the literature [44–48]. According to Gholizadeh-Vayghan and Rajabipour [46] free swelling and water absorption of ASR products are increased at Ca/Si values of 0.23–0.37. ASR products presented in this paper are in this range. The type of alkali in ASR products: sodium or potassium, is probably influenced by the external access of sodium chloride solution, therefore an increased content of sodium ions is observed compared to potassium in specimens exposed to AAR-12 test conditions. This is not observed in the specimens after AAR-11 exposure. A similar dependence of the chemical composition of ASR products on the external access of alkali was found in [47]. In most currently studied specimens, mainly amorphous reaction products were found. According to Leemann [49], the amorphous gel may have much greater expansion capacity than the crystalline gel. And it is the amorphous products that are responsible for the initial cracking of the aggregate.

In comparison to concrete specimens subjected to RILEM AAR-11 test conditions, those tested with alkali supply exhibited not only abundant presence of ASR products but also larger cracks in granite grains and in cement paste, with ASR products filling cracks up to 80 µm wide. Observed differences in crack system development were

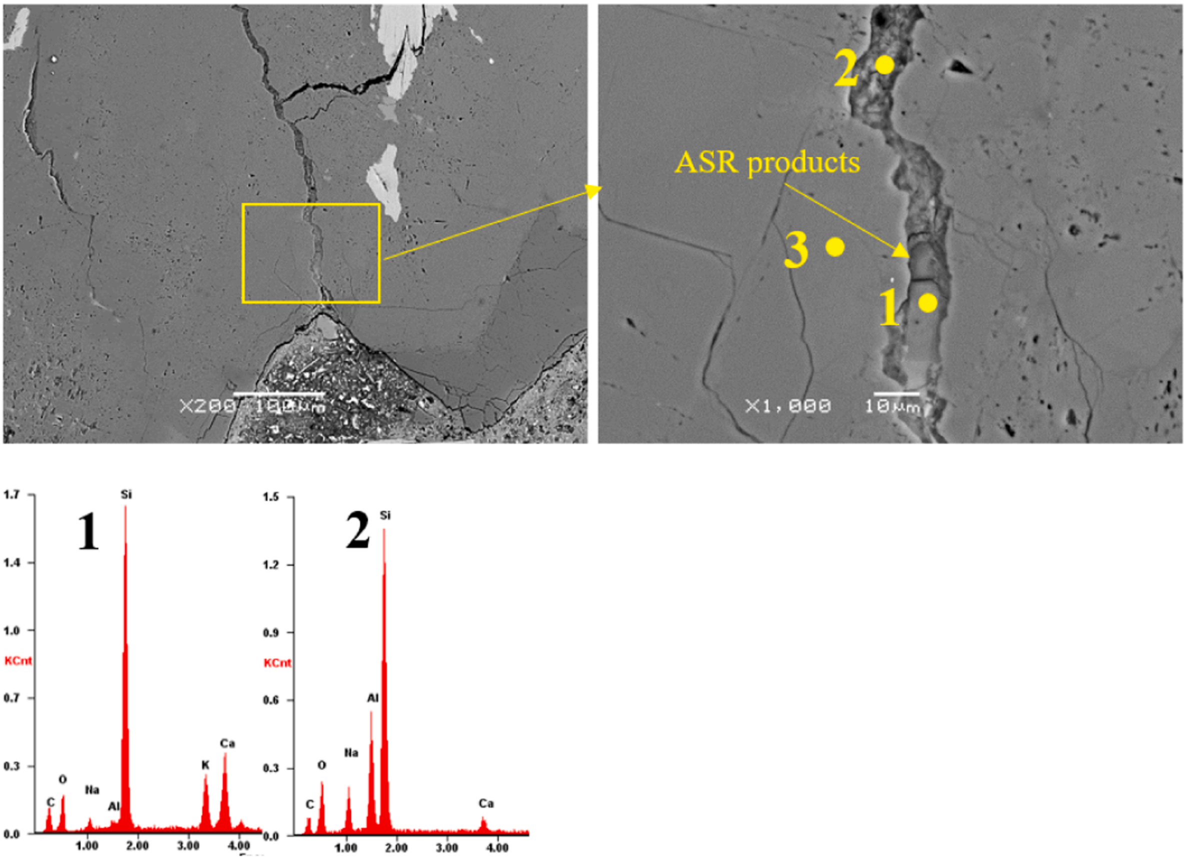

Fig. 14. Amorphous ASR products in granite grain (1) in concrete HA-HR after AAR-11 test exposure, (2) sodium-calcium feldspar.

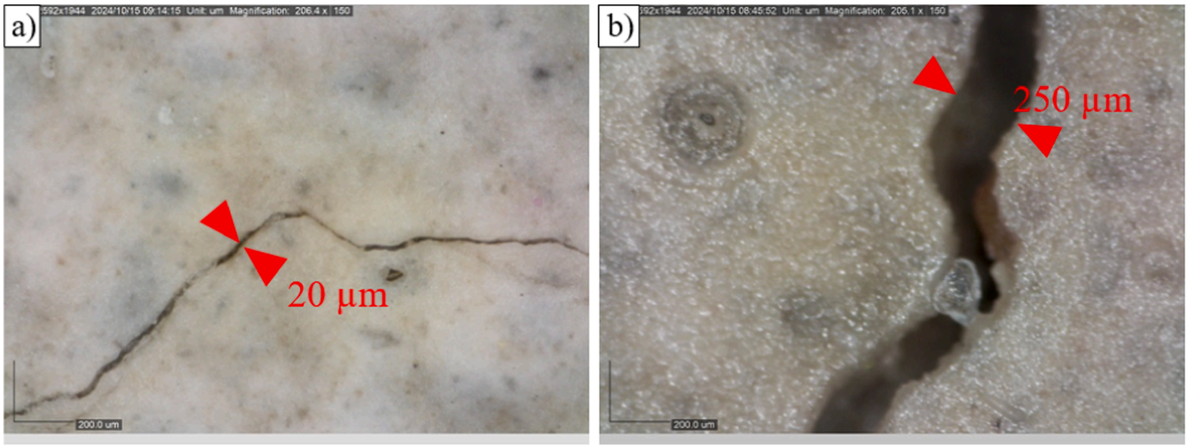

Fig. 15. Surface cracking on concrete prisms after AAR-11 (a) and AAR-12 (b) tests, specimens with the highest final expansion.

Table 7
Reactivity Index (RI) determined according to ATT method.

Alkali content Na_2O_{eq} [kg/m^3]	1.30	2.45	3.17	4.32	5.25
RI	0.73 ± 0.48	1.18 ± 0.18	1.43 ± 0.33	1.79 ± 0.04	1.58 ± 0.01

associated with changes in elastic properties of concrete. As shown in Fig. 20a the influence of alkali loading on the relative change of dynamic elastic modulus of concrete was found negligible for the standard 60°C exposure without alkali supply, i.e. the relative changes were less than 5 %. With alkali supply conditions (Fig. 20b) the E_{dyn} reduction is clearly enhanced with the increase of alkali loading in concrete. Such a trend is close to a linear trend within a major part of alkali loading range. The rate of E_{dyn} reduction is not significantly influenced by the degree of reactivity of sand. A lack of correlation of expansion development with E_{dyn} changes was previously noted by Reinhardt and Mielich [50] for fog chamber exposure of concrete specimens, i.e. with no alkali supply. However, during RILEM AAR-12 testing reported in [51] such a correlation was found and beneficial effects of ground granulated blastfurnace slag or fly ash used as components of cement were consistently demonstrated as reduced changes in resonance elastic modulus with exposure time. E_{dyn} determination seems meaningful only for an elevated degree of cracking observed during alkali supply conditions.

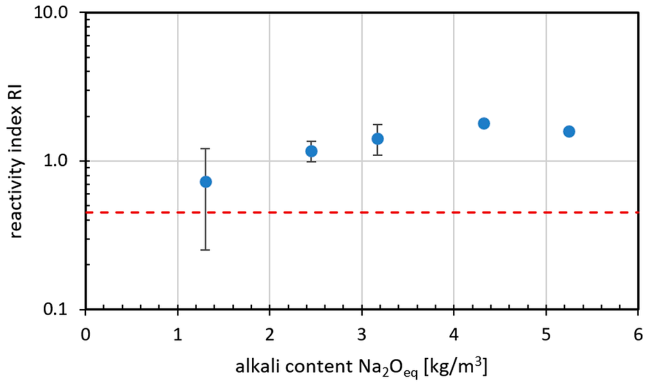

Fig. 16. Reactivity index for coarse granite aggregate vs alkali content for determining the AT according to the AASHTO standard procedure [35].

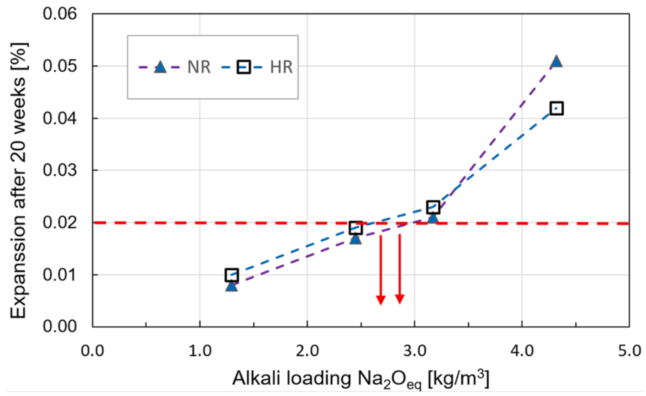

Fig. 17. Influence of alkali loading on the final expansion of concrete specimens exposed to 60°C temperature and 100 % RH environmental conditions (RILEM AAR-11 test exposure).

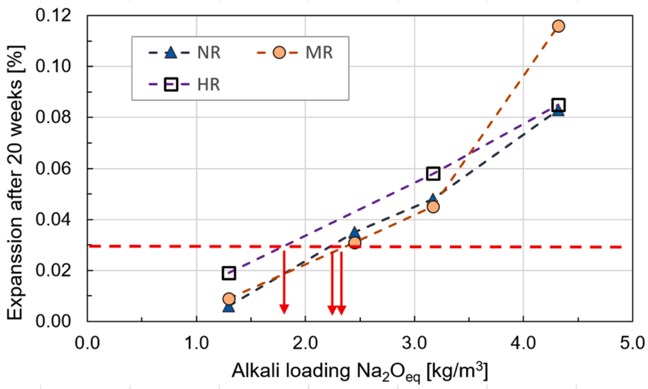

Fig. 18. Influence of alkali loading on the final expansion of concrete specimens exposed to cyclic variation of temperature (from 20 to 60 °C), moisture (drying or 100 % RH) and soaking in 3 % NaCl solution (RILEM AAR-12 test exposure).

The temperature and relative humidity conditions inside concrete specimens subjected to AAR-12 test procedure have not been previously investigated. Moisture is a critical factor for the development of the ASR. The moisture needed for the ASR development has been prominently measured by numerous researchers using the RH. A context for obtained RH data evaluation can be found in [52] that revealed the influence of different external relative humidity conditions on the expansion kinetics. So called RH threshold was found decreasing with the

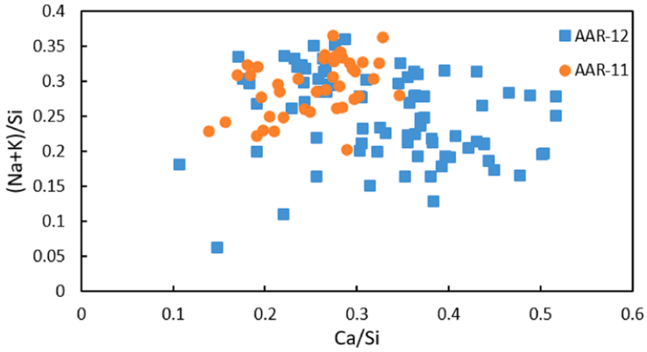

Fig. 19. Characteristics of ASR products composition ((Na+K)/Si vs Ca/Si atomic ratios) in cracked granite aggregate after RILEM AAR-12 and AAR-11 exposure.

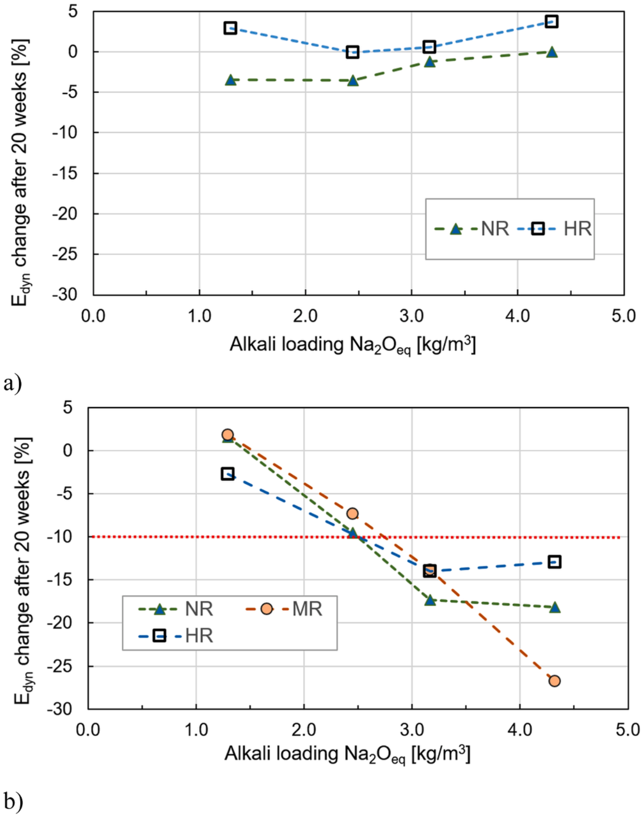

Fig. 20. Influence of alkali loading on the relative change of dynamic elastic modulus of concrete specimens exposed to: a) 60 °C temperature and 100 % RH environmental conditions (RILEM AAR-11 procedure); b) cyclic variation of temperature (from 20 to 60 °C), moisture (drying, 100 % RH) and soaking in 3 % NaCl solution (RILEM AAR-12 test conditions).

temperature increase, i.e. between 80 % and 85 % for a 20°C, about 75 % at 38°C and below 59 % at 60°C. However, the pore water saturation in concrete in known to change non-linearly with relative humidity in concrete and small variation in saturation can lead to important differences in ASR expansion [53]. RH is a useful indicator of moisture content in concrete, although doesn't directly measure the moisture content. Therefore some researchers [40] have argued that the degree of water saturation is a better means of moisture threshold evaluation.

The limitations of this study are related mainly to the significance of reactivity criteria, that have been established for laboratory test specimens using the derived correlations with either field observations of test blocks or cores taken from structural elements subjected to service conditions. The performance of concrete exposed to service conditions is influenced by a combination of local atmospheric conditions, service loads (e.g. road traffic) and maintenance treatments, like deicing salts sprinkled onto the surface in winter seasons. Sodium chloride is being used either as rock salt for de-icing or as salt brine for anti-icing, but its effective use is limited to the temperature of −9.4 °C [54]. Although possible alkali silica-reaction will rather take place during warm months, sodium and chloride ions from NaCl solutions might penetrate into concrete and remain in its pore solution. According to [55–57], such a combination of aggressive factors, including thermal gradients and mechanical fatigue action results in microcracking build-up, enhances the penetration of alkaline solutions from the surface into concrete skin. The microcracking associated with the dynamic E-modulus decreased by about 10–15 % was found sufficient [55] to promote the transport of moisture and harmful ions inside specimens. A pH increase in concrete pore solution resulting from the dissolution of $Ca(OH)_2$ in the presence of sodium chloride is considered as the cause for the exacerbation of ASR [38]. With a multitude of possible combinations environmental/service loads, types of deicers and frequency of their use the applied criterion for ASR development and AT determination cannot be universal. This is in contrast with just atmospheric exposure to alkaline media, like seawater aerosols, that did not indicate exacerbating ASR in concrete [58]. There is a need for elaborating the ASR trigger criteria for various climate and road service conditions, preferably via modelling considering the alkali concentration in pore solution and correlation with outdoor exposure monitoring [59].

5. Conclusions

Performed experimental tests on Portland cement concrete with granite coarse aggregate containing both microcrystalline quartz and strained quartz, combined with natural siliceous sand as fine aggregate, resulted in the following conclusions.

1. At simulated pavement environments with external alkali supply the alkali threshold for ASR expansion of concrete containing moderately reactive granite aggregate is from 1.8 to 2.3 kg/m^3 Na_2O_{eq}. AT is found sensitive to potential reactivity of sand in the aggregate blends- it is reduced by about 0.5 kg/m^3 Na_2O_{eq} when reactive sand is used instead of nonreactive sand.
2. At high humidity exposure conditions without alkali supply AT is 2.7–2.9 kg/m^3 Na_2O_{eq} and it is found insensitive to the potential reactivity level of sand. The change of exposure conditions to simulated pavement environments results in the relative reduction of AT by 0.5 or 1 kg/m^3 Na_2O_{eq} depending on the sand reactivity level.
3. In contrast to merely amorphous alkali-silica reaction products observed in concrete at high humidity exposure without alkali supply, both crystalline and amorphous products were present at simulated pavement environments with external alkali supply. The composition of alkali-silica reaction products characterized by (Na+K)/Si ratio was not significantly influenced by the environmental exposure conditions. For amorphous ASR products higher Ca/Si ratios were observed under AAR-12 than AAR-11, mostly in the range 0.29–0.37 and 0.26–0.30, respectively.
4. The change of dynamic elastic modulus of concrete subjected to simulated pavement environments is found sensitive to the alkali loading in concrete and is associated with higher expansion, more extensive and wider cracking in both aggregate and cement paste. Therefore ΔE_{dyn} could be a practical indicator of ASR-induced damage development in unreinforced pavement slabs, potentially useful for the pavement service life evaluation.

CRediT authorship contribution statement

Aneta Brachaczek: Writing – review & editing, Writing – original draft, Visualization, Validation, Methodology, Investigation, Formal analysis, Data curation, Conceptualization. **Mariusz Dąbrowski:** Investigation. **Paweł Lisowski:** Investigation. **Kinga Dziedzic:** Investigation. **Michal A. Glinicki:** Writing – review & editing, Writing – original draft, Supervision, Methodology, Conceptualization.

Declaration of Competing Interest

The authors declare that they have no known competing financial interests or personal relationships that could have appeared to influence the work reported in this paper

Acknowledgements

The 4th author acknowledges the financial support for her investigation by Polish National Science Centre as part of Preludium Project no. 2023/49/N/ST8/02157. The insightful comments and discussions provided by anonymous Reviewers are greatly appreciated.

Appendix 1

Monitoring of internal hydrothermal conditions in concrete specimens during RILEM AAR-12 exposure

A1.1. Test set-up

To enable the temperature and humidity measurements inside concrete, four holes of 20 mm in diameter at were drilled into prismatic specimens to the designed depth (1/4 and 1/2 of the specimen thickness) as shown schematically in Fig. A1. Rigid plastic tubes were inserted into the holes and sealed with flexible adhesive. Two chambers were used for iButton miniature data loggers placement [34], two other chambers for Vaisala probes placement [33]. The Vaisala Humidity and Temperature Probe HMP44 with a measurement range of 0 … 100 %RH; −40 … + 80°C and ± 1.5 %RH accuracy was used. For data acquisition the Vaisala Handheld Humidity and Temperature Meter HM40 was applied. The iButton DS1923 Hygrochron Temperature/Humidity Data Loggers (the operating range: −20°C to +85°C; 0–100 %RH) were used. Data was stored in the internal memory until the sensor removal and then was transferred to a computer through the serial 1-Wire protocol.

The principal assumption for the setup design was the identical air volume inside the measurement chambers for both types of measuring devices, thus the length of tubes was adjusted accordingly. The iButton sensors were placed in tightly sealed copper fittings, securely connected to the installed tubes. Continuous measurements of temperature and relative humidity of air inside the measurement chambers were conducted at 15 minutes intervals during the full test cycle lasting two weeks.

Measurements with the Vaisala probe were not conducted continuously but only at selected time slots within the AAR-12 timeline (otherwise the chambers were sealed with rubber stoppers). These time slots were selected mostly at specimen transfer stages when an easy access to the specimen was available without significantly affecting the prevailing hydrothermal conditions (Fig. A2):

- on day “0”: at laboratory room temperature prior to placing the specimen in the drying cabinet,
- on day “1”: after the first day in the drying cabinet,
- on day “5”: after five days in the drying cabinet,
- on day "5.125": just before immersion in the 3 % NaCl solution,
- on day “7”: after removal from the NaCl solution following two days of immersion,
- on day “14”: at the end of test cycle - after six days in condensate reactor, followed by one day of temperature stabilization at laboratory room conditions.

Each reading was preceded by a 30-minute stabilization period inside the measurement tube after inserting the Vaisala sensor. External measurements were conducted with the Vaisala probe in a tube of the same diameter and length, firmly attached to the concrete surface on Day "0" – before placing the sample in the dryer.

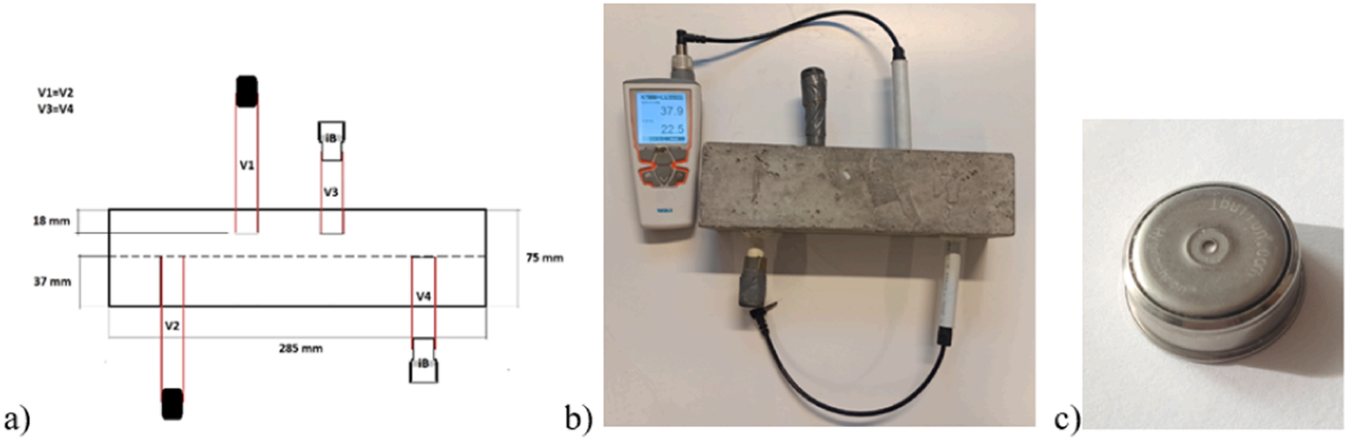

Fig. A1. Test set up for monitoring the temperature and humidity inside concrete: a) the location and depth of drilled holes, location of glued measurement chambers, b) an actual view of a specimen two Vaisala probes in measurement chambers, iButtons inside closed measurement chambers not visible, c) iButton sensor

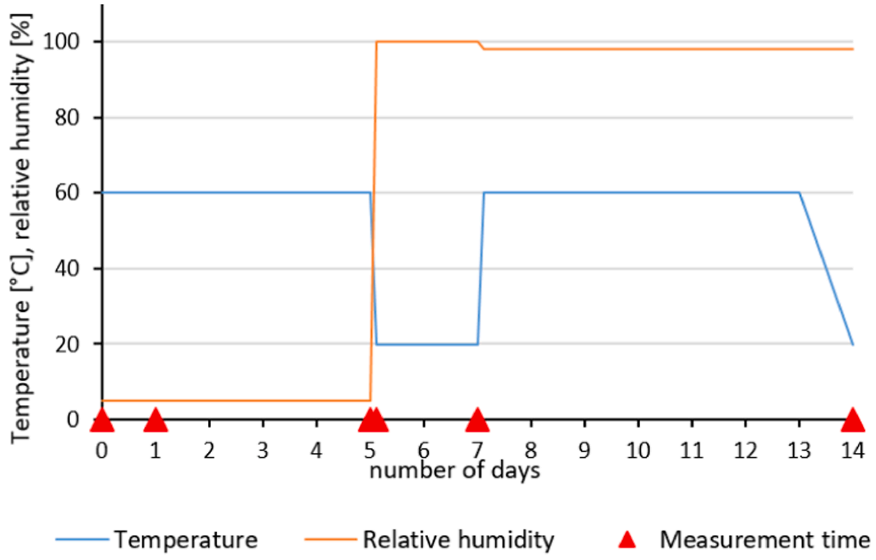

Fig. A2. Selected time slots for measurements using Vaisala probe during the full specimen exposure cycle as per RILEM AAR-12

A1.2. Results of measurements

The recorded internal temperature and relative humidity in concrete during two weeks period at the depth of 18 mm and 37 mm is shown in Fig. A3 and in Fig. 4 in main text, respectively. The temperature measurements obtained with iButton sensors demonstrate the expected changes during the four stages of exposure. Recorded temperature history at the depth of 1/4 and 1/2 of the specimen thickness is well fitting the specified temperature limits.

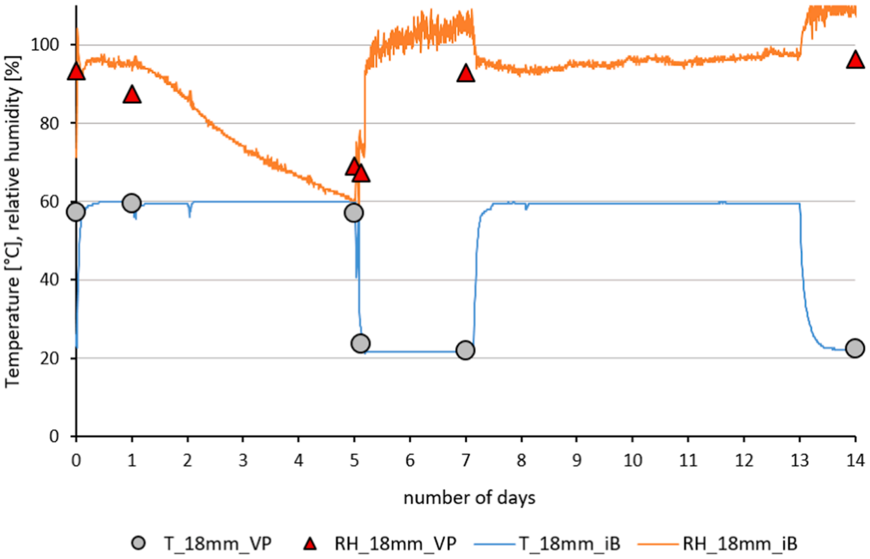

Fig. A3. Temperature and relative humidity in concrete at the depth of 18 mm recorded during the first test cycle of RILEM AAR-12 procedure (VP-Vaisala probe, iB-iButton)

The RH measurements at the depth of 37 mm (Fig. 4 in main text) demonstrate a gradual RH decrease during drying phase, from 90 % to 95 % down to about 80 %, subsequent rapid increase during the immersion phase and levelling off in the range 90–98 %. During the transition from NaCl solution the RH is reduced to about 90 % and later it very slowly increases up to 98 %. The prevailing RH during the specimen storage in the container in condensate reactor is within the range 94–97 %. The closed container transition from the 60 °C reactor to 22°C laboratory environment resulted in data out of the range of measurements. Similar observations were made in respect to measurements performed at the depth closer to the specimen surface (Fig.A3), but the changes induced by drying and soaking were relatively stronger. That resulted in RH data out of the range of measurements during soaking stage and final stage of container storage at laboratory conditions.

The sensors failed to provide the full humidity history but RH data acquired during the first test cycle can be partly accepted. The sensors failed to register accurately the RH levels when exposed to water vapor saturation exceeding the dew point, until the sensor had dried. Due to sensor defects under conditions of full air saturation with water vapor their use for measurements during subsequent exposure cycles was compromised.

In measurements taken by Vaisala probes during the drying stage the RH reduces from 95 % to about 65–69 %, during the soaking stage goes up to 95 % and the end of the cycle stays at the level of 97 %. No significant influence of the depth of measurements were found. The Vaisala probe measurements provide an accurate assessment of rate of internal humidity changes in concrete throughout test cycle. Temperature measurements by Vaisala probes are well in accordance with iButton records. No doubts are raised in respect to obtained temperature data.

Data availability

Data will be made available on request.

References

[1] A. Leemann, R. Rezakhani, E. Gallyamov, P. Lura, R. Zboray, M. Griffa, M. Shakoorioskooie, Z. Shi, R. Dähn, G. Geng, E. Boehm-Courjault, S. Barbotin, K. Scrivener, B. Lothenbach, M. Bagheri, J.F. Molinari, Alkali-silica reaction – a multidisciplinary approach, RILEM Tech. Lett. 6 (2022) 169–187, https://doi.org/10.21809/rilemtechlett.2021.151.

[2] M.A.T.M. Broekmans, Deleterious reactions of aggregate with alkalis in concrete, Rev. Mineral. Geochem. 74 (2012) 279–364, https://doi.org/10.2138/rmg.2012.74.7.

[3] D. Constantiner, S. Diamond, Alkali release from feldspars into pore solutions, Cem. Concr. Res. 33 (2003) 549–554, https://doi.org/10.1016/S0008-8846(02)01001-3.

[4] E. Menéndez Méndez, A. Santos Silva (Editors) Total Alkalis in Concrete—Contribution to Alkali-silica Reaction. State-of-the-Art Report of the RILEM Technical Committee 258-AAA WP3, Springer 2025.

[5] R. Helmuth, D. Stark, S. Diamond, M. Moranville-Regourd, Alkali–Silica Reactivity: An Overview of Research. Report SHRP-C-342. Strategic Highway Research Program, National Research Council, Washington, D.C., 1993.

[6] H.F.W. Taylor, A method for predicting alkali ion concentrations in cement pore solutions, Adv. Cem. Res. 1 (1987) 5–17, https://doi.org/10.1680/adcr.1987.1.1.5.

[7] R.D. Hooton, M.D.A. Thomas, T. Ramlochan, Use of pore solution analysis in design for concrete durability, Adv. Cem. Res. 22 (2010) 203–210, https://doi.org/10.1680/adcr.2010.22.4.203.

[8] T.F. Rønning, B.J. Wigum, J. Lindgard, P. Nixon, I. Sims, Recommendation of RILEM TC 258-AAA: RILEM AAR-0 outline guide to the use of RILEM methods in the assessment of the alkali-reactivity potential of concrete, Mater. Struct. 54 (2021) 206, https://doi.org/10.1617/s11527-021-01687-w.

[9] P. Rivard, M.-A. Bérubé, J.-P. Ollivier, G. Ballivy, Alkali mass balance during the accelerated concrete prism test for alkali-aggregate reactivity, Cem. Concr. Res. 33 (2003) 1147–1153, https://doi.org/10.1016/S0008-8846(03)00020-6.

[10] J. Lindgård, Ö. Andiç-Çakır, I. Fernandes, T.F. Rønning, M.D.A. Thomas, Alkali–silica reactions (ASR): Literature review on parameters influencing laboratory performance testing, Cem. Concr. Res. 42 (2012) 223–243, https://doi.org/10.1016/j.cemconres.2011.10.004.

[11] R.G. Sibbick, C.L. Page, Threshold alkali contents for expansion of concretes containing British aggregates, Cem. Concr. Res. 22 (1992) 990–994, https://doi.org/10.1016/0008-8846(92)90123-D.

[12] I. Sims, United Kingdom and Ireland, in: Alkali-Aggregate Reaction in Concrete: A World Review, Edited By Ian Sims, Alan Poole, CRC Press 2017, pp. 167-276.

[13] ASTM C 1778- 22 Standard Guide for Reducing the Risk of Deleterious Alkali-Aggregate Reaction in Concrete.

[14] EN 197-1: 2012 Cement – composition, specifications and conformity criteria for common cements.

[15] T.F. Rønning, B.J. Wigum, J. Lindgard, Recommendation of RILEM TC 258-AAA: RILEM AAR-10: determination of binder combinations for non-reactive mix design using concrete prisms–38 °C test method, Mater. Struct. 54 (2021) 204, https://doi.org/10.1617/s11527-021-01679-w.

[16] J.F. Muñoz, C. Balachandran, T.S. Arnold, New Chemical Reactivity Index to Assess Alkali–Silica Reactivity, J. Mater. Civ. Eng. 33 (2021) 04021037, https://doi.org/10.1061/(ASCE)MT.1943-5533.0003640.

[17] AASHTO TP 144 -23 Standard Method of Test for Determining the Potential Alkali-Silica Reactivity of Coarse Aggregates (TFHRC-TFAST), American Association of State and Highway Transportation Officials..

[18] E. Coppens, Alkali concentration of cement pore solution and its relation with alkali-silica reaction, Constr. Build. Mater. 411 (2024) 134285, https://doi.org/10.1016/j.conbuildmat.2023.134285.

[19] Y. Zhang, X. Xu, Q. Zhao, J. Chang, S. Ding, X. Liu, C.S. Poon, Long-term investigation of alkali-silica reaction behaviors in seawater sea-sand concrete, Cem. Concr. Compos 151 (2024) 105611, https://doi.org/10.1016/j.cemconcomp.2024.105611.

[20] I. Borchers, Recommendation of RILEM TC 258-AAA: RILEM AAR-12: determination of binder combinations for non-reactive mix design or the resistance

to alkali-silica reaction of concrete mixes using concrete prisms – 60 °C test method with alkali supply, Mater. Struct. 54 (2021) 202, https://doi.org/10.1617/s11527-021-01681-2.

[21] C. Müller, I. Borchers, E. Eickschen, Experience with ASR test methods: advice on obtaining practical evaluation criteria for performance testing and aggregate testing, Cem. Int 11 (2013) 86–93.

[22] C. Giebson, K. Seyfarth, H.M. Ludwig, Influence of sodium chloride on ASR in highway pavement concrete. In: H.M. Bernardes, N.P. Hasparyk, eds. 15th International Conference on Alkali-Aggregate Reaction, 3-7 July 2016, Sao Paulo, Brazil (2016).

[23] R. Przondziono, J.J. Timothy, F. Weise, E. Krütt, R. Breitenbücher, G. Meschke, M. Hofmann, Degradation in concrete structures due to cyclic loading and its effect on transport processes - Experiments and modeling, Struct. Concr. 18 (2017) 519–527, https://doi.org/10.1002/suco.201600180.

[24] M.A. Glinicki, K. Bogusz, D. Jóźwiak-Niedźwiedzka, M. Dąbrowski, ASR performance of concrete at external alkali supply - effects of aggregate mixtures and blended cement, Int. J. Pavement Eng. 24 (2023), https://doi.org/10.1080/10298436.2023.2171038.

[25] ASTM C 1260-23 Standard Test Method for Potential Alkali Reactivity of Aggregates (Mortar-Bar Method).

[26] GDDKiA (2019) Wytyczne techniczne klasyfikacji kruszyw krajowych i zapobiegania reakcji alkalicznej w betonie stosowanym w nawierzchniach dróg i drogowych obiektach inżynierskich, Generalna Dyrekcja Dróg Krajowych i Autostrad (Technical guidelines for the classification of domestic aggregates and the prevention of alkaline reaction in concrete used in road pavements and road engineering structures – in Polish). 〈https://www.gov.pl/web/gddkia/reaktywnosc-kruszyw〉.

[27] EN 206:2022 Concrete - Specification, performance, production and conformity.

[28] EN 1097–6:2013 Tests for mechanical and physical properties of aggregates. Determination of particle density and water absorption.

[29] EN 196-2: 2013 Method of testing cement. Chemical analysis of cement.

[30] ASTM C114 -18 Standard Test Methods for Chemical Analysis of Hydraulic Cement.

[31] I. Borchers, J. Lindgard, T.F. Rønning, B.J. Wigum, Recommendation of RILEM TC 258-AAA: RILEM AAR-11: determination of binder combinations for non-reactive mix design or the resistance to alkali-silica reaction of concrete mixes using concrete prisms - 60 °C test method, Mater. Struct. 54 (2021) 203, https://doi.org/10.1617/s11527-021-01680-3.

[32] ASTM C215-19 Standard Test Method for Fundamental Transverse, Longitudinal, and Torsional Resonant Frequencies of Concrete Specimens.

[33] W. Kubissa, M.A. Glinicki, Influence of internal relative humidity and mix design of radiation shielding concrete on air permeability index, Constr. Build. Mater. 147 (2017) 352–361, https://doi.org/10.1016/j.conbuildmat.2017.04.177.

[34] M.A. Glinicki, R. Jaskulski, M. Dąbrowski, Design principles and testing of internal frost resistance of concrete for road structures-critical review, Roads Bridges - Drog. i Mosty 15 (2016) 21–43, https://doi.org/10.7409/rabdim.016.002.

[35] AASHTO T 416-24 Standard Method of Test for the Determination of Alkali-Threshold for Alkali-Silica Reactivity of in Aggregates used in Concrete (ATT), American Association of State Highway and Transportation Officials, Washington DC.

[36] A. Leemann, C. Merz, An attempt to validate the ultra-accelerated microbar and the concrete performance test with the degree of AAR-induced damage observed in concrete structures, Cem. Concr. Res. 49 (2013) 29–37, https://doi.org/10.1016/j.cemconres.2013.03.014.

[37] W.J. McCoy, O.L. Eshenour, Significance of total and water-soluble alkali contents of portland cement, J. Mater. 3 (1968) 684–694.

[38] I. Borchers, Leistungsbasiertes Konzept für einen ausreichenden AKR-Widerstand von Beton, Dissertation zur Erlangung des Doktorgrades der Ingenieurwissenschaften, Technischen Universität Clausthal, 01.08.2023.

[39] G. Plusquellec, M.R. Geiker, J. Lindgård, J. Duchesne, B. Fournier, K. De Weerdt, Determination of the pH and the free alkali metal content in the pore solution of concrete: Review and experimental comparison, Cem. Concr. Res. 96 (2017) 13–26.

[40] J. Lindgård, M.D.A. Thomas, E.J. Sellevold, B. Pedersen, Ö. Andiç-Çakır, H. Justnes, T.F. Rønning, Alkali–silica reaction (ASR)—performance testing: Influence of specimen pre-treatment, exposure conditions and prism size on alkali leaching and prism expansion, Cem. Concr. Res. 53 (2013) 68–90, https://doi.org/10.1016/j.cemconres.2013.05.017.

[41] A. Brachaczek, M.A. Glinicki, T. Manninger, S. Krispel, Comparative ASR performance of concrete at external alkali supply, in: L.F.M. Sanchez, C. Trottier (Eds.), ICAAR 2024, RILEM Bookseries 49, Springer Nature, 2024, pp. 266–274, https://doi.org/10.1007/978-3-031-59419-9_31.

[42] B. Savija, E. Schlangen, J. Pacheco, S. Millar, T. Eichler, G. Wilsch, Chloride ingress in cracked concrete: A laser induced breakdown spectroscopy (LIBS) study, in: J. Adv. Concr. Technol, 12, 2014, pp. 425–444, https://doi.org/10.3151/jact.12.425.

[43] S. Millar, G. Wilsch, T. Eichler, C. Gottlieb, H. Wiggenhauser, Laser Induced Breakdown Spectroscopy (LIBS) im Bauwesen – automatisierte Baustoffanalyse, Beton- und Stahlbetonbau 110 (2015) 501–510, https://doi.org/10.1002/best.201500030.

[44] E. Boehm-Courjault, S. Barbotin, A. Leemann, K. Scrivener, Microstructure, crystallinity and composition of alkali-silica reaction products in concrete determined by transmission electron microscopy, Cem. Concr. Res. 130 (2020) 105988, https://doi.org/10.1016/j.cemconres.2020.105988.

[45] A. Leemann, Z. Shi, J. Lindgård, Characterization of amorphous and crystalline ASR products formed in concrete aggregates, Cem. Concr. Res. 137 (2020) 106190, https://doi.org/10.1016/j.cemconres.2020.106190.

[46] A. Gholizadeh-Vayghan, F. Rajabipour, The influence of alkali–silica reaction (ASR) gel composition on its hydrophilic properties and free swelling in contact with water vapor, Cem. Concr. Res. 94 (2017) 49–58, https://doi.org/10.1016/j.cemconres.2017.01.006.

[47] A. Antolik, D. Jóźwiak-Niedźwiedzka, ASR induced by chloride- and formate-based deicers in concrete with non-reactive aggregates, Constr. Build. Mater. 400 (2023) 132811, https://doi.org/10.1016/j.conbuildmat.2023.132811.

[48] H.E. Joo, Y. Takahashi, Analytical and experimental studies on alkali-silica reaction mechanism: Aggregate cracking and chemical composition change of gel, Cem. Concr. Compos 139 (2023) 105003, https://doi.org/10.1016/j.cemconcomp.2023.105003.

[49] A. Leemann, Alkali-silica reaction - sequence, products and possible mechanisms of expansion, Proc. 16th Int. Conf. Alkali-Aggregate React. Concr. Lisbon, Part. 2 (2022).

[50] H.W. Reinhardt, O. Mielich, Static vs. dynamic Young's modulus as indicator for ASR degradation, International RILEM Conference on Advances in Construction Materials Through Science and Engineering, Editor(s): Christopher Leung and K.T. Wan, RILEM Publications SARL, 2011, 411-418.

[51] K. Bogusz, M.A. Glinicki, Volumetric stability and elastic properties of concrete subjected to simulated service exposure conditions on road pavements, Cem. Wapno Beton 27 (2022) 410–424, https://doi.org/10.32047/CWB.2022.27.6.4.

[52] S. Poyet, A. Sellier, B. Capra, G. Thèvenin-Foray, J.-M. Torrenti, et al., Influence of water on alkali-silica reaction: experimental study and numerical simulations, J. Mater. Civ. Eng. 18 (4) (2006), https://doi.org/10.1061/(ASCE)0899-1561(2006)18:4(588).

[53] O..Olajide, M. Nokken, L. Sanchez, A Review on the Role of Moisture and Temperature in Alkali-Silica Reaction (ASR). Proc. 16th Int. Conf. on Alkali-Aggregate Reaction in Concrete (ICAAR), Lisbon, Portugal, 2022.

[54] G. Xu, X. Shi, Impact of Chemical Deicers on Roadway Infrastructure: Risks and Best Management Practices, in: Sustainable Winter Road Operations, Xianming Shi and Liping Fu (eds.), John Wiley & Sons, Hoboken, NJ, 2018, 211-240.

[55] R. Breitenbücher, S. Kunz, Influences of cyclic loadings on the properties of pavement concrete, Airfield and Highway Pavement 2013: Sustainable and Efficient Pavements - Proceedings of the 2013 Airfield and Highway Pavement Conference, 2013, pp. 214–224.

[56] A. Wiedmann, F. Weise, E. Kotan, H.S. Müller, B. Meng, Effects of fatigue loading and alkali–silica reaction on the mechanical behavior of pavement concrete, Struct. Concr. 18 (2017) 539–549, https://doi.org/10.1002/suco.201600179.

[57] F. Weise, J. von Werder, T. Manninger, B. Maier, M. Fladt, S. Simon, A. Gardei, D. Hoehnel, S. Pirskawetz, B. Meng, A multiscale and multimethod approach to assess and mitigate concrete damage due to alkali–silica reaction, Adv. Eng. Mater. 24 (2022) 2101346, https://doi.org/10.1002/adem.202101346.

[58] M.D.A. Thomas, E.G. Moffatt, The Performance of Concrete in a Marine Environment, Sixth International Conference on Durability of Concrete Structures, Paper Number PL01, 18 - 20 July 2018, Leeds, UK.

[59] T.N. Nguyen, L.F.M. Sanchez, J. Li, B. Fournier, V. Sirivivatnanon, Correlating alkali-silica reaction (ASR) induced expansion from short-term laboratory testings to long-term field performance: a semi-empirical model, Cem. Concr. Compos 134 (2022) 104817, https://doi.org/10.1016/j.cemconcomp.2022.104817.